Acridine–O6-benzylguanine hybrids: Synthesis, DNA binding, MGMT inhibition and antiproliferative activity

Jaime Franco Pinto, Alexandra Fillion, Patricia Duchambon, Sophie Bombard, Anton Granzhan

Acridine–O^6-benzylguanine hybrids: Synthesis, DNA binding, MGMT inhibition and antiproliferative activity

Jaime Franco Pinto,[a,b] Alexandra Fillion,[a,b] Patricia Duchambon,[a,b] Sophie Bombard [a,b,*] and Anton Granzhan [a,b,*]

[a] CNRS UMR9187, Inserm U1196, Institut Curie, PSL Research University, 91405 Orsay, France; [b] CNRS UMR9187, Inserm U1196, Université Paris Saclay, 91405 Orsay, France

E-mail: sophie.bombard@curie.fr; anton.granzhan@curie.fr

ABSTRACT

O^6-Methylguanine-DNA-methyltransferase (MGMT) is a key DNA repair enzyme involved in chemoresistance to DNA-alkylating anti-cancer drugs such as Temozolomide (TMZ) through direct repair of drug-induced O^6-methylguanine residues in DNA. MGMT substrate analogues, such as O^6-benzylguanine (BG), efficiently inactivate MGMT *in vitro* and in cells; however, these drugs failed to reach the clinic due to adverse side effects. Here, we designed hybrid drugs combining a BG residue covalently linked to a DNA-interacting moiety (6-chloro-2-methoxy-9-aminoacridine). Specifically, two series of hybrids, encompassing three compounds each, were obtained by varying the position of the attachment point of BG (N^9 of guanine vs. the O^6-benzyl group) and the length and nature of the linker. UV/vis absorption and fluorescence data indicate that all six hybrids adopt an intramolecular stacked conformation in aqueous solutions in a wide range of temperatures. All hybrids interact with double-stranded DNA, as clearly evidenced by spectrophotometric titrations, without intercalation of the acridine ring and do not induce thermal stabilization of the duplex. All hybrids, as well as the reference DNA intercalator (6-chloro-2-methoxy-9-aminoacridine **8**), irreversibly inhibit MGMT *in vitro* with variable efficiency, comparable to that of BG. In a multidrug-resistant glioblastoma cell line T98G, benzyl-linked hybrids **7a–c** and the N^9-linked hybrid **19b** are moderately cytotoxic (GI_{50} ≥ 15 μM after 96 h), while N^9-linked hybrids **19a** and **19c** are strongly cytotoxic (GI_{50} = 1–2 μM), similarly to acridine **8** (GI_{50} = 0.6 μM). Among all compounds, hybrids **19a** and **19c**, similarly to BG, display synergic cytotoxic effect upon co-treatment with subtoxic doses of TMZ, with combination index (CI) values as low as 0.2–0.3. In agreement with *in vitro* results, compound **19a** inactivates cellular MGMT but, unlike BG, does not induce significant levels of DNA damage, either alone or in combination with TMZ,

as indicated by the results of γ-H2AX immunostaining experiments. Instead, and unlike BG, compound **19a** alone induces significant apoptosis of T98G cells, which is not further increased in a combination with TMZ. These results indicate that molecular mechanisms underlying the cytotoxicity of **19a** and its combination with TMZ are distinct from that of BG. The strongly synergic properties of this combination represent an interesting therapeutic opportunity in treating TMZ-resistant cancers.

1. INTRODUCTION

Glioblastoma multiforme (GBM) is the most common primary brain cancer in adults worldwide. It is one of the deadliest cancers and is still contemplated as incurable. The survival time for more than 90% of patients is only 15 to 18 months, whereas only 0.47% of patients survive for more than 5 years. Its hallmarks are genomic instability, rapid cellular proliferation, diffuse infiltration and several multiresistance factors [1–3]. Its current palliative and invasive treatments consist in tumor removal, followed by radiotherapy in combination with the lipophilic prodrug temozolomide (TMZ) [1]. TMZ is able to cross the blood–brain barrier (BBB) and spontaneously decomposes at neutral or slightly basic pH, yielding the highly reactive methyldiazonium cation. This monoalkylating agent is responsible for the alkylation of several macromolecules, chiefly DNA [1,4]. Three major modified nucleobases include N^3-methyladenine (N^3MeA) and N^7-methylguanine (N^7MeG), representing 70% and 9% of DNA alkylation damage, respectively, as well as O^6-methylguanine (O^6MeG) formed in a 5% yield [1,4]. Despite being a minor product, the latter is responsible for the major DNA damage response in the cell. Its similarity with adenine, in terms of lipophilicity and hydrogen bond donor / acceptor pattern, leads to the insertion of a thymine facing the modified nucleobase in the newly synthesized DNA strand during the first replication cycle. The resulting O^6MeG:T mismatch is recognized by the DNA mismatch repair system (MMR) that removes the newly inserted base (i.e., dT). This base insertion / removal process is repeated in a futile cycle leading to the replication fork stalling and cell cycle arrest in the G_2/M phase that carries the cell death by numerous pathways [1,5]. Regardless the mechanisms leading to cell death, 50% of patients that receive TMZ chemotherapy show refractivity to it. It was shown that the major mechanism responsible for this resistance is the overexpression of the O^6-methylguanine-DNA-methyltransferase (MGMT), a suicide enzyme that reacts with O^6MeG in DNA in an irreversible fashion by removing the methyl group and restoring the former guanine residue, allowing the cell to survive and replicate [1,4,6]. One of the strategies designed to defeat TMZ resistance relies on the use of MGMT inhibitors, or more precisely MGMT inactivators that represent substrate analogues that covalently and irreversibly react with the Cys residue of the enzyme leading to its deactivation. Among these, O^6-benzylguanine (BG, Chart 1) and O^6-(3-bromothenyl)guanine, or Lomeguatrib (LG), represent the most studied examples. Both compounds were shown to enhance TMZ activity in numerous *in vitro* experiments with different cell lines, but failed in the Phases I–II of clinical trials [7].

Since it has been shown that GBM presents a large genetic heterogeneity and many factors contribute to its resilient characteristics [1,3,4,8], another strategy that could be employed is the design of small molecules that could play a multitarget effect, aiming to circumvent the tumor resistance [3]. In other types of cancer a similar concept, relying on the use of so-called

hybrid molecules, has been employed at least in the early stages of drug discovery [9,10]. By definition, hybrid drugs contain two different pharmacophore units that can amplify or modulate each other's activity, displaying a dual activity inside a cell. With regard to MGMT inhibitors, the BG moiety was exploited in the design of a hybrid drug MR30 by linking to a quinazoline derivative targeting the epidermal growth factor receptor (EGFR) in A549 cell lines [11]. In parallel, BG has been linked to DNA-alkylating nitrosourea derivatives; the resulting hybrid drugs showed markedly increased cytotoxicity with regard to clinically used nitrosoureas or their combinations with BG in several human glioma cells lines such as SF126, SF763 or SF767 [12,13]. Finally, BG scaffold has also been attached to the caged methyltriazene in prodrugs that release both DNA-methylating agents and BG upon hydrolysis. These prodrugs were more active than TMZ in a large panel of cancerous cell lines, demonstrating the power of the hybrid drug approach [14].

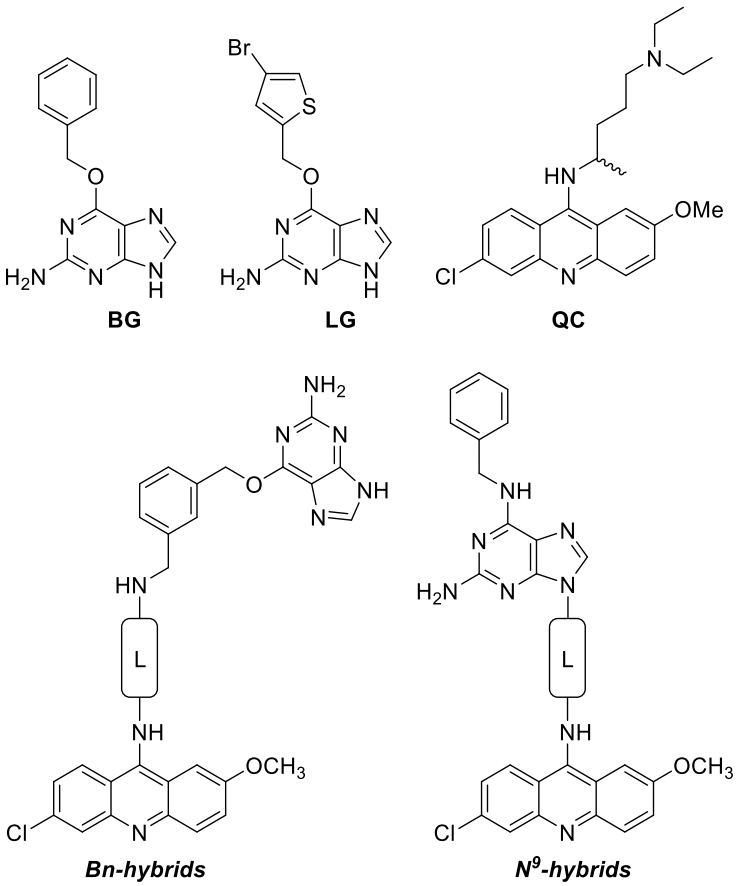

Chart 1. Structures of *O*^{6}-benzylguanine (BG), Lomeguatrib (LG), quinacrine (QC), and two types of BG–acridine hybrids (Bn-hybrids and *N*^{9}-hybrids) studied in this work. L = linker.

DNA-binding compounds, in particular those that intercalate into DNA, represent an old and well-established class of anti-cancer agents [15–17]. In addition to their well-established,

DNA-related anti-cancer activities stemming from the inhibition of DNA/RNA polymerases and topoisomerases [17–20], 9-aminoacridine derivatives, such as quinacrine (QC, Chart 1), recently regained increased interest due to their low genotoxicity and "curaxin" activity [21], that is, tumor-specific cytotoxicity stemming from the activation of expression of the tumor suppressor protein p53, namely through inhibition of NF-κB via chromatin trapping of the FACT (facilitates chromatin transcription) complex [18,22–26]. Moreover, the acridine fragment has been extensively exploited in the design of hybrid drugs targeting malaria [27] and DNA repair inhibitors targeting apurinic/apyrimidinic (AP) sites in the DNA [28–30], as well as trinucleotide $(CUG)_n$ or tetranucleotide $(CCUG)_n$ RNA repeats in Myotonic Dystrophy Type 1 (DM1) or Type 2 (DM2), respectively [31,32]. Additionally, the strong fluorescence properties of acridine derivatives enable their visualization in cells by fluorescence microscopy, allowing the evaluation of cellular uptake, sub-cellular distribution and metabolism of the drugs.

On these premises, we designed two series of BG–acridine hybrids connected through a linker (L) attached either at the benzyl ring (Bn-hybrids) or at N^9 position of BG (N^9-hybrids), respectively (Chart 1). In this work we present the synthesis of these drugs, evaluation of their DNA-binding properties and inhibition of MGMT activity *in vitro* and in cells, as well as evaluation of cytotoxic properties of these compounds alone and in combination with TMZ in a multidrug-resistant glioma cell line (T98G) [33–36].

2. RESULTS

2.1. Chemistry

The structural details of MGMT in the complex with inhibitors [6], as well as the data on *in vitro* inhibitory activity of BG derivatives [37–40] and *in silico* docking experiments [41] suggest that, within the BG scaffold, positions 3 and 4 of the benzyl ring, as well as N^9 of the guanine have minimal impact on the binding and reaction with the enzyme. These positions were exploited to design two series of hybrid molecules presented on Chart 1. Notably, these two types of hybrids are expected to produce different outcomes upon reacting with MGMT: in the case of Bn-hybrids, a reaction with MGMT would lead to a transfer of the acridine residue to the enzyme through a process reminiscent of SNAP-Tag labelling [42], resulting in a deactivated enzyme endowed with a DNA-intercalating tag. In the case of N^9-hybrids, the enzymatic reaction should result in benzylation of MGMT, leaving a debenzylated acridine–guanine conjugate as a potential DNA-binding drug.

Synthesis of Bn-hybrids: In the design of this series, the linker was introduced through an amide function at position 3 of the benzyl ring of BG. Indeed, it was reported that 3-

aminomethyl-BG **5** (Scheme 1) is a much more potent MGMT inhibitor than BG due to the formation of additional hydrogen bonds with the enzyme [38]. The synthesis of Bn-hybrids was performed by formation of the amide bond linking 3-aminomethyl-BG and carboxy derivatives of acridine as the final step (Scheme 1).

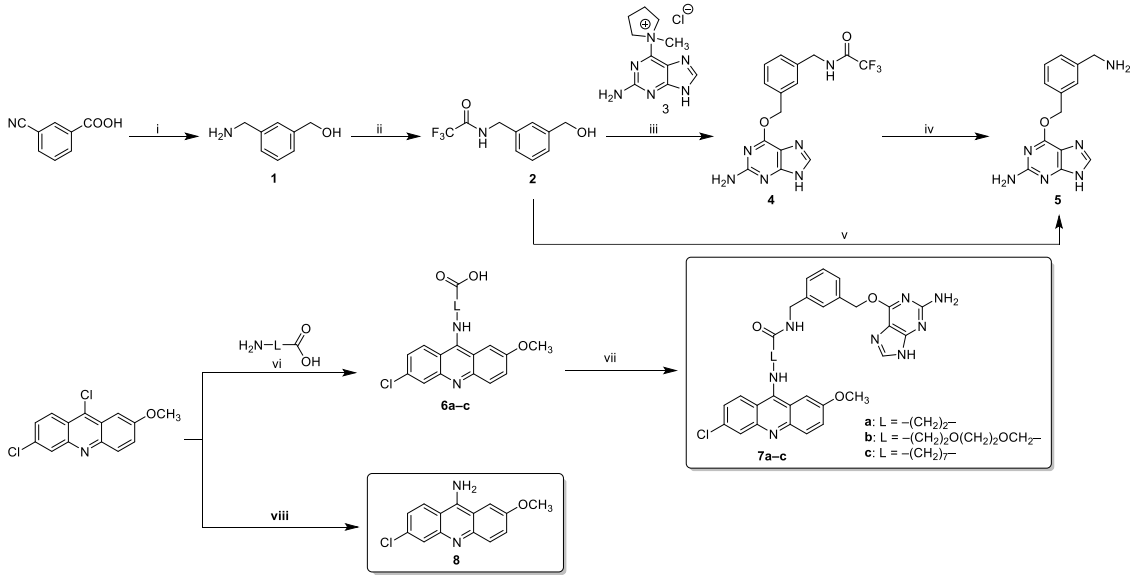

Scheme 1. Synthesis of Bn-hybrids **7a–c** and the reference compound **8**. Reagents and conditions: i) BH_3•THF, THF, 0 °C to room temp., 24 h, 98%; ii) CF_3CO_2Et, NEt_3, MeOH, 0 °C to room temp., 2 h, 67%; iii) *t*-BuOK, DMF, room temp., 5 h, 48%; iv) K_2CO_3, MeOH/H_2O, reflux, 4 h, 51%; v) a) *t*-BuOK, pyridine, room temp., 48 h, b) H_2O, reflux, 2 h, 77% in one pot; vi) a) PhOH, 70 °C, 1 h; b) H_2N-L-COOH, 110 °C, 3 h, 89%, 98% and 94% for **6a**, **6b** and **6c** respectively; vii) **5**, HBTU/HOBt, DIPEA, DMF, 0 °C to room temp., 24 h, 34%, 62%, 65% for **7a**, **7b** and **7c** respectively; viii) a) PhOH, 70 °C, 1 h; b) $(NH_4)_2CO_3$, 110 °C, 3 h, 81%.

3-Aminomethyl-BG **5** was obtained using a previously reported strategy [38,43]. Thus, the reduction of 3-cyanobenzoic acid with THF-BH_3 gave in an excellent yield the amino alcohol **1**, which was immediately protected as a trifluoroacetamide **2** in a good yield. This derivative was made to react with the activated guanine **3** in basic conditions (*t*-BuOK, DMF) to yield the benzylated compound **4** in a moderate yield (48%), comparable to that described the literature [13,38]. Basic hydrolysis of **4** allowed to obtain compound **5** in a moderate yield (51%). In order to improve the yield of this compound, a one-pot synthesis was attempted, where a reaction of **2** with the activated guanine **3** in pyridine (48 h, room temperature) was followed by addition of water and heating to reflux for 2 h. This way, compound **5** was obtained in a 77% yield, representing a significant improvement over the previously published procedures.

The acridine-derived carboxylic acids **6a–c** were obtained in excellent yields through activation of 9,6-dichloro-2-methoxyacridine by heating in phenol, followed by the addition of the commercially available ω-aminoacids [44–46]. Coupling of the acid **6a** with the amine **5** using EDCI/HOBt (72 h) allowed to obtain the product **7a** in low yield (19%); an improved yield of this product (34%) was obtained using HBTU/HOBt reagent pair (24 h). These conditions were also employed for the synthesis of hybrids **7b** and **7c**, obtained in good yields (62% and 65%, respectively). Finally, 9-amino-6-chloro-2-methoxyacridine **8** was prepared as a reference compound through ammonolysis of 9,6-dichloro-2-methoxyacridine (Scheme 1).

Synthesis of N^9-hybrids: Initially, N^9-alkylation of 6-chloroguanine with 4-(*N*-Boc-amino)butyl bromide **9** in basic conditions was performed (Scheme 2). After deprotection of the terminal amino group in compound **10** in acidic conditions (HCl / dioxane), a reaction with the activated acridine derivative **11** was performed in typical condition (PhOH, 110 °C), aiming to obtain compound **12**. However, products **13** and **14** were obtained instead (in 24% and 16% yields, respectively), presumably due the nucleophilic substitution of the chlorine atoms by phenol and residual water respectively. Therefore, another strategy was also chosen were BG was alkylated at N^9 position with the building block **9** to yield the product **15** in a moderate yield (46%). A deprotection in acidic conditions followed by a reaction with acridine **11** was performed aiming to obtain compound **19a**; unfortunately, the concomitant debenzylation led to compound **16** once again in a moderate yield. Since the benzyl substituent at the O^6 position of guanine appeared to be acid-sensitive [47], a third route was explored. Thus, BG was alkylated with the commercially available ω-(bromoalkyl)phthalimides **16a–b** or with the iodo derivative **16c** [48] in basic conditions, to give the intermediates **17a–c** in good yields. After the removal of the phthalimide group by hydrazinolysis, the free primary amines **18a–c** were obtained in excellent yields (above 80%) [12]. Finally, a nucleophilic substitution reaction with extemporarily prepared phenoxyacridine **11** (pyridine, reflux) yielded the desired hybrids **19a–c** in moderate yields [31,32].

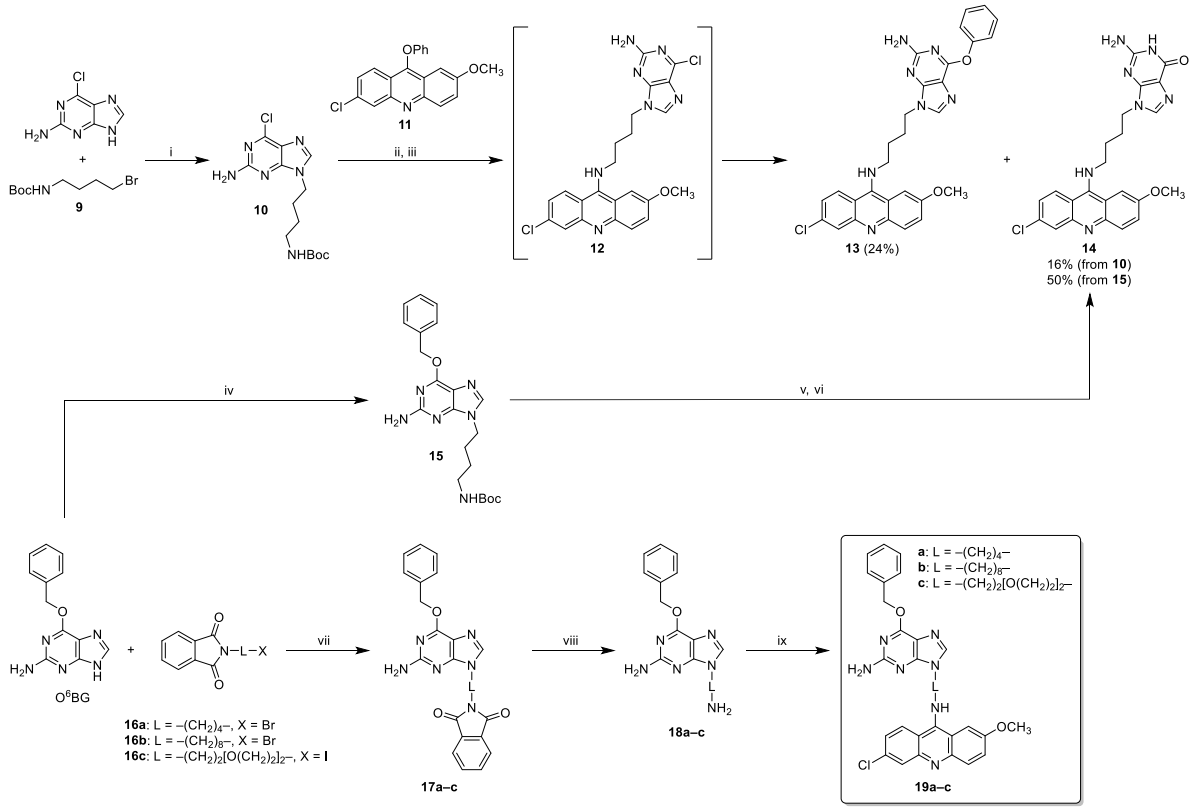

Scheme 2. Synthesis of N^9-hybrids **19a–c**. Reagents and conditions: i) Cs_2CO_3, DMF, room temp., 24 h, 40%; ii) HCl, dioxane, 0 °C to room temp., 4 h; iii) **11**, PhOH, 110 °C, 6 h and then 18 h, room temp; iv) **9**, Cs_2CO_3, DMF, room temp., 24 h, 46%; v) HCl, dioxane, 0 °C to room temp., 4 h; vi) **11**, PhOH, 110 °C, 4 h and then 20 h, room temp, 50%; vii) Cs_2CO_3, DMF, room temp., 24 h (**17a**) or 0 °C, 8 h and then 16 h, room temp (**17b**, **17c**), 68–94%; viii) $N_2H_4 \cdot H_2O$, EtOH, 65 °C, 1-2.5 h 82–94%; ix) **11**, pyridine, reflux, 24 h, 20–59%.

2.2. Self-stacking of BG–acridine hybrids and interaction with ds DNA

Photophysical properties of the hybrids: Conjugates of 9-aminoacridine with nucleic acid bases are known to adopt predominantly an intramolecular self-stacked (folded) conformation in aqueous solutions, which is characterized by hypochromism of the acridine chromophore [49,50]. To evaluate the intrinsic conformation of acridine–BG hybrids, we studied their photophysical properties in several solvents in comparison with reference compounds, acridine **8** and BG (Figure 1 and Figure S1). In diluted (c = 10 μM) aqueous solutions, both the long-wavelength (350–475 nm) and short-wavelength (250–300 nm) absorption bands of the hybrids were red-shifted (by 3–20 nm) and significantly weaker comparing with those of acridine **8**, giving evidence of intramolecular stacking (Figure 1). The values of hypochromism (H, %), i.e., the ratio of the oscillator strength of the hybrids to the sum of those of reference compounds **8** and BG (Table 1), provide a semi-quantitative measure of this effect [49,50]. In

aqueous solutions, Bn-hybrids **7b** and **7c** were most prone to self-stacking (*H* = 60 and 77%, respectively), in contrast to their short-linker analogue **7a** (*H* = 27%). This is in contrast to what was observed in the series of acridine–nucleobase conjugates, where short (e.g., C_3) linkers were shown to promote the highest degree of intramolecular stacking, and can be explained by a model where the attachment of the linker through the benzyl residue leads to the stacking of the latter with the acridine ring instead of the guanine moiety, as suggested by molecular modelling (Figure S2). In the series of N^9-hybrids, the short-linker derivative **19a** expectedly showed the highest degree of self-staking (*H* = 48%); of note, the analysis of compound **19b** was approximative due to its poor aqueous solubility. To evaluate the efficiency of the intramolecular stacking, we recorded absorption spectra of the hybrids in aqueous solutions at varied temperatures (20 to 75 °C). No significant changes were observed in this temperature range (Figure S3), indicating the high stability of the folded conformation [49]. However, self-staking was significantly reduced in organic solvents (MeOH, MeCN, THF), except for compound **7c** that showed high hypochromism even in these conditions (Table 1).

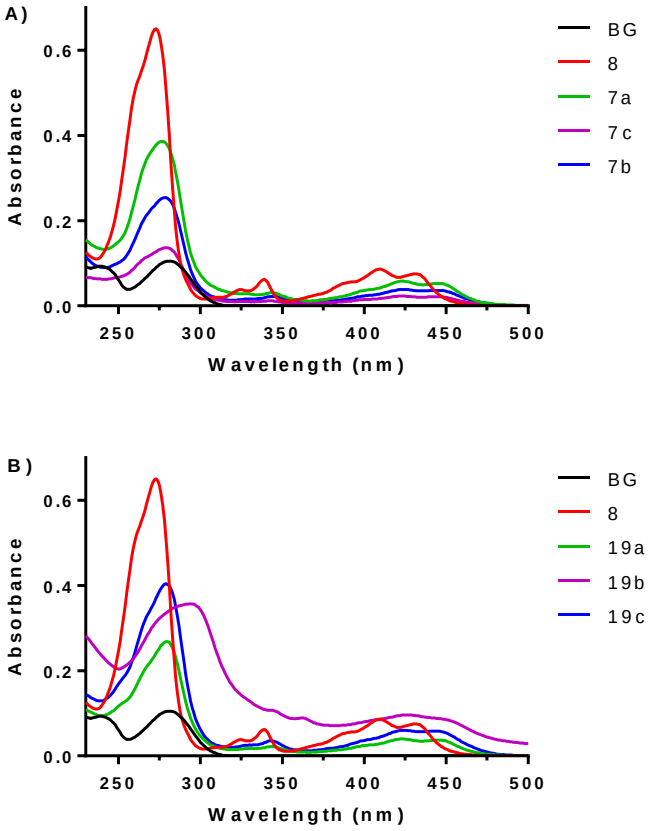

Figure 1. Absorption spectra of A) *Bn*-hybrids and B) N^9-hybrids, BG and acridine **8** in water (*c* = 10 µM). Compound **19b** was not fully soluble in these conditions.

Table 1. Photophysical properties of compounds.

Compound	Hypochromism (*H*, %)[a]				Fluorescence quantum yield (*Φ*)[b]			
	THF	MeCN	MeOH	H_2O	THF	MeCN	MeOH	H_2O
8					0.22	0.22	0.42	0.36
7a	31	15	8	27	0.12 *(0.55)*	0.06 *(0.27)*	0.07 *(0.17)*	0.08 *(0.22)*
7b	38	50	49	60	0.06 *(0.27)*	0.05 *(0.23)*	0.06 *(0.14)*	0.01 *(0.03)*
7c	67	63	61	77	0.06 *(0.27)*	0.04 *(0.18)*	0.06 *(0.14)*	0.01 *(0.03)*
19a	44	34	36	48	0.09 *(0.41)*	0.07 *(0.32)*	0.06 *(0.14)*	0.01 *(0.03)*
19b	5	6	0	13	0.08 *(0.36)*	0.09 *(0.41)*	0.05 *(0.12)*	0.05 *(0.14)*
19c	0	12	6	36	0.09 *(0.41)*	0.09 *(0.41)*	0.06 *(0.14)*	< 0.01 *(< 0.03)*

[a] Calculated from absorption spectra, recorded at c = 10 μM (Figure 1 and Figure S1). [b] From fluorescence spectra recorded at c = 1 μM; quantum yield reference: Coumarin 153 (Φ = 0.38) [51]. The values in parentheses are the ratios of the quantum yield of the compound to that of acridine **8** in the same solvent.

Fluorescence spectra of compounds (Figure S4) further confirmed the intramolecular stacking in aqueous solutions, since the fluorescence of hybrids was strongly quenched (from 4.6-fold for **7a** up to > 700-fold in the case of **19c**), comparing with acridine **8** (Table 1). In organic solvents, the quenching effect of the BG moiety was much less pronounced. Altogether, these results confirm that self-stacking properties of acridine–BG hybrids can be modulated by the attachment mode of the two moieties (Bn vs. N^9 attachment) and the length of the linker, with Bn-hybrids **7b** and **7c** showing most the stable folded conformation.

Interaction with DNA: The folded conformation could influence the DNA-binding properties of the hybrids, since the binding to a non-damaged, fully matched DNA duplex would require the opening of the folded form to allow the intercalation of the acridine ring. The DNA-binding properties of the compounds were initially studied by spectrophotometric titrations with calf thymus DNA (CT DNA, Figure S5) [52]. In the case of all hybrids, addition of CT DNA led to a further decrease of the intensity of the long-wavelength absorption bands without concomitant red shift; the latter was observed only in the case of acridine **8** behaving as a typical

intercalator (Figure S5, D). The values of dissociation constants (K_d, Table 2), determined by non-linear fitting of binding isotherms (Figure 2), indicate that the DNA affinity of the hybrids (K_d = 13 to 23 µM) was not dramatically different with respect to acridine **8** (K_d = 16.1 µM). These results indicate that, independently on the attachment mode and the length of the linker connecting the two moieties, all hybrids interact with double-stranded DNA.

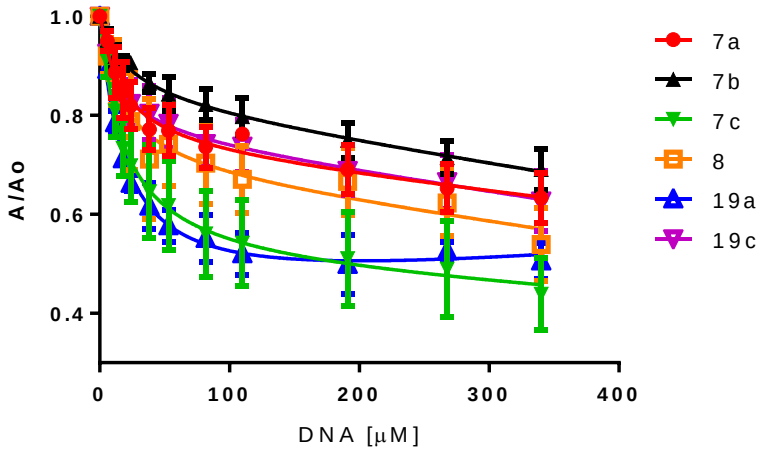

Figure 2. Titration isotherms for spectrophotometric titrations of CT DNA to solutions of compounds (c = 20 µM in 10 mM $LiAsO_2Me_2$, 100 mM KCl buffer, pH 7.2). Data are means ± s.d. from at least three independent experiments. Lines represent the fitting of experimental data to the one-site binding model, with K_d values given in Table 2.

Table 2. DNA-binding properties of compounds, obtained from spectrophotometric titrations and thermal denaturation experiments with calf thymus (CT) DNA.

Compound	K_d / µM [a]	ΔT_m / °C [b]
7a	16.2 ± 6.3	1.5 ± 1.1
7b	23.4 ± 8.8	–0.7 ± 0.7
7c	14.3 ± 6.1	0.2 ± 0.5
8	16.1 ± 8.7	8.5 ± 0.6
19a	19.1 ± 2.9	0.6 ± 1.0
19b	ND	0.7 ± 0.6
19c	13.4 ± 5.4	–1.4 ± 1.2

[a] Binding constants, obtained from spectrophotometric titrations presented in Figure 2. Data are means ± s.d. from three replicates. [b] Ligand-induced shift of melting temperature of CT DNA; conditions: c(CT DNA) = 12.5 µM, c(cpd) = 6.25 µM in 10 mM $KAsO_2Me_2$, pH 7.2.

The interaction of the drugs with CT DNA was also studied through thermal denaturation experiments, which provide a measure of ligand-induced stabilization of the DNA duplex through a shift of a melting temperature (ΔT_m). The results (Table 2) indicate that acridine **8** strongly stabilized CT DNA (ΔT_m = 8.5 °C); in contrast, none of hybrids induced significant effect on the thermal stability of CT DNA. In order to explore the discrepancy between the results of spectrophotometric titration that clearly give evidence of interaction of hybrids with DNA and the absence of thermal stabilization effects, we performed ethidium bromide (EB) displacement assay (Figure S6). While acridine **8** efficiently displaced bound EB, as demonstrated by the concentration-dependent decrease of fluorescence intensity with a DC_{50} value (corresponding to the displacement of 50% of bound EB) of ~ 8 μM, none of hybrids was able to displace EB, giving evidence of the absence of intercalative binding to DNA. Furthermore, induced circular dichroism (CD) spectra of DNA–ligand complexes supported the differences in the binding modes. While compound **8** displayed a positive induced CD band in the region corresponding to the long-wavelength transition band of acridine (360–460 nm), characteristic for DNA intercalators and similar to what has been reported for 9-aminoacridine [53], hybrid **19a** did not show induced CD signal in the same region (Figure S7).

2.3. *In vitro* MGMT inhibition

In order to study the efficiency of compounds to inhibit MGMT activity, an *in vitro* coupled enzymatic assay was performed [54–56]. In this gel electrophoresis-based assay, the activity of MGMT is monitored through the cleavage of a fluorescently labeled 26-bp DNA oligonucleotide by restriction endonuclease (Bsp119I), that can occur only after demethylation of the O^6MeG residue within the restriction site (5′-TT^C(O^6MeG)AA-3′ / 5′-TT^CGAA-3′) by MGMT (Figure 3, A and Figure S8). A first comparative analysis was performed using the drug concentration of 12.5 μM and a reaction time of 5 min. A control assay was performed to verify the effect of the compounds on the activity of the Bsp119I endonuclease in the conditions of the coupled assay (Figure S8); none of the compounds was found to inhibit this enzyme to a significant extent (> 4%), confirming that, in the conditions of the coupled assay, the observed effect was exclusively due to MGMT inhibition.

In the coupled assay, reference inhibitors BG and LG inhibited MGMT activity by 25% and 94%, respectively (black bars in Figures 3, B). In the series of Bn-hybrids, the inhibitory activity of compounds **7a** and **7b** was comparable to that of BG (around 21% of inhibition), whereas compound **7c** proved to be significantly more potent (47% inhibition). In the series of N^9-hybrids, compounds **19a** and **19b** showed the inhibitory efficiency similar to that of BG (18% and 23% inhibition, respectively), while compound **19c** proved to be the least efficient with

only 5% inhibition. Among other compounds, 3-aminomethyl-BG **5** inhibited the enzyme by 43%, in agreement with its previously documented higher activity than BG [38], whereas N^9-substituted BG derivatives **17a** and **18a** inhibited the enzyme by 22% and 37%, respectively. Unexpectedly, acridine **8** revealed to be a strong MGMT inhibitor, inhibiting 48% of enzymatic activity. Likewise, acridine hybrids **13** and **14**, lacking the benzyl moiety and thus unable to react with MGMT via a benzyl transfer, also inhibited the enzymatic activity by 15% and 16%, respectively (Figure 3, B and Figure S8). Consequently, for the hybrid derivatives it is difficult to determine which part of the molecules (BG, acridine, and/or both) contribute to their MGMT inhibitory effect.

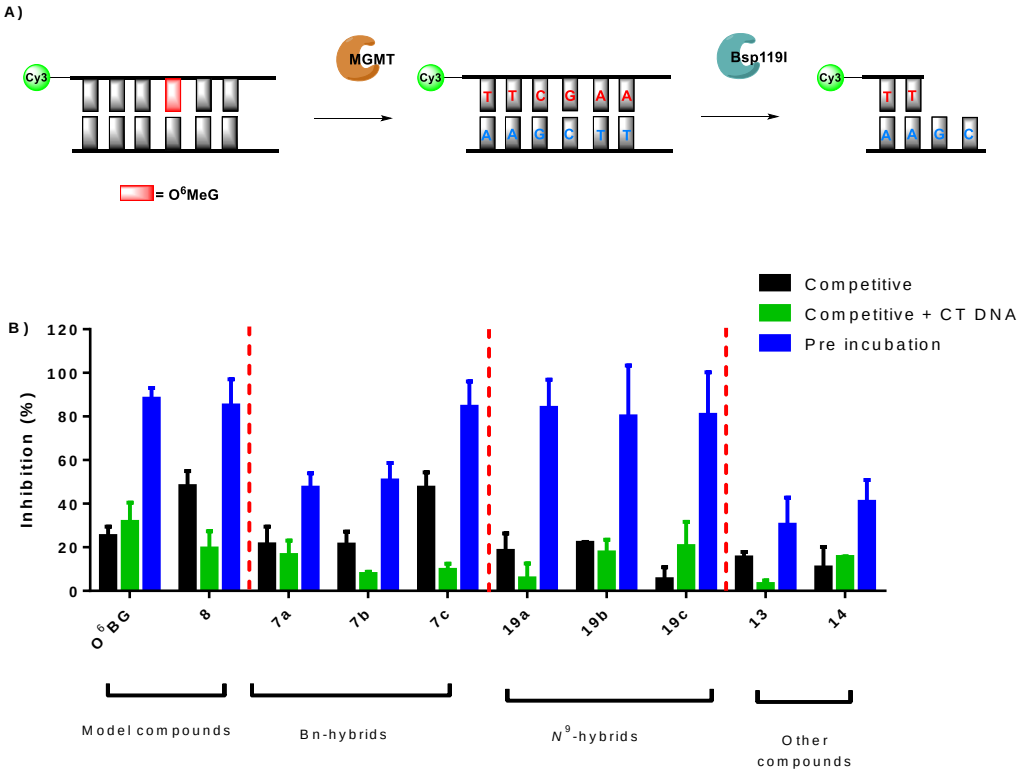

Figure 3. *In vitro* inhibition of MGMT activity. A) Principle of the coupled enzymatic assay. B) Comparison of MGMT inhibition observed in coupled assay performed in standard conditions (black bars), in the presence of calf thymus DNA (40 µM base pairs, green bars), and upon 30-min preincubation of compounds with the enzyme (blue bars). In all cases, *c*(inhibitor) = 12.5 µM, *c*(substrate) = 200 nM, *c*(MGMT) = 800 nM, *c*(Bsp119I) = 0.2 U mL^{-1}. Data are means ± s.d. from at least three experimental replicates.

In order to prove irreversible inhibition of MGMT by the hybrids, another assay was performed by preincubating the enzyme and the drugs for 30 min prior to addition of the substrate (blue

bars in Figure 3, B). As expected, pre-incubation increased the inhibitory efficiency of BG from 25 to 88%, giving evidence of irreversible inhibition. In the case of acridine **8** pre-incubation also increased the inhibitory effect (from 48 to 85%), also suggesting an irreversible inhibition; this may be due to a reaction of acridine with the enzyme, or a non-specific inhibition mechanism [57]. The same effect, i.e., an increase of inhibitory activity up to ~80%, was observed for all hybrids except **7a** and **7b**, whose activity reached only ~50% inhibition in this setting. The lower activity of both derivatives in fact agrees with their stronger intrinsic self-stacking properties (as evidenced by higher hypochromism values, cf. Table 1) that render both parts of the molecule less available for interaction with the enzyme. Conversely, in the case of **7c** and **19a–b**, it is difficult to attribute the increase of inhibition activity observed upon pre-incubation with the enzyme to irreversible inhibition by BG or acridine moieties of the hybrid.

Finally, to evaluate the effect of DNA binding on the inhibitory activity of the hybrids, we assayed the activities in the presence of 40 µM (base pairs) CT DNA, i.e., non-substrate DNA (green bars in Figure 3, B). In the case of BG, the inhibitory activity was slightly increased in the presence of CT DNA (from 25 to 31%), in agreement with previous reports [58], whereas for acridine **8** it was reduced from 47% to 20%, a fact that can be explained by partial sequestration of the compound by DNA. In the case of the hybrid drugs, the inhibitory activity of compound **19c** was increased from 5 to 21%, following the trend of BG. For the other drugs, the level of inhibitory activity was either maintained (**7a**, **14** and **19b**) or reduced (**7b**, **7c**, **13** and **19a**) in the presence of CT DNA; again, the reduction of inhibitory activity can be interpreted as partial sequestration of the inhibitor by non-substrate DNA. The fact that MGMT inhibitory activity is mostly maintained in the presence of CT DNA indicates that these compounds may be potent in cellular conditions.

2.4. Antiproliferative properties

Intrinsic cytotoxicity: The cytotoxicity of six BG–acridine conjugates **7a–c** and **19a–c**, as well as the derivatives **13** and **14** and three reference compounds (BG, **5**, and acridine **8**) was assessed in a multidrug-resistant glioblastoma cell line T98G [33–35] using CellTiter-Glo® assay, that provides a measure of viability of the cells through the ATP-dependent luminescent signal [59]. Cells were treated with the compounds for 96 h and GI_{50} values, i.e., concentration of the compound leading to 50% inhibition of viability with respect to compound vehicle (0.5% v/v DMSO) were determined (Table 3; dose-response curves: Figure S9). As was expected for an MGMT-expressing cell line, TMZ was poorly active ($GI_{50} \approx 375$ µM), in agreement with literature reports [4,35,36].

Table 3. Cytotoxicity of the synthesized compounds in T98G cells upon 96-h incubation.

Compound	GI_{50} (μM)[a]
reference compounds	
TMZ	≈ 375
acridine **8**	0.6 ± 0.1
BG and derivatives	
BG	91.8 ± 8.1
5	> 25
17a	> 25
18a	> 25
Bn-hybrids	
7a	15.6 ± 104
7b	≈ 25
7c	19.4 ± 1.3
N^9-hybrids	
19a	1.1 ± 0.1
19b	14.5 ± 0.2
19c	2.1 ± 0.3
Other hybrids	
13	0.8 ± 0.1
14	> 25

[a] Values are means ± s.d. from at least three biological replicates. The studied range of concentrations was 0 to 750 μM for TMZ, 0 to 600 μM for BG, and 0 to 50 μM for other drugs due to solubility limitations.

The data presented in Table 3 give a first idea on the structure–properties relationships in BG–acridine conjugates. First of all, BG showed a relatively low cytotoxicity (GI_{50} = 91.8 μM), in agreement with the published results obtained in different cancerous cell lines (e.g., GI_{50} > 100 μM at 24 h in HT-29 cells) [12,13,40,60]. Likewise, BG derivatives substituted in the benzyl ring (**5**) or at the N^9 atom, but devoid of the acridine fragment (**17a** and **18a**) showed low cytotoxicity (viability ≥ 70% at a concentration 25 μM). Instead, acridine **8** showed the highest activity of all evaluated compounds with a GI_{50} = 0.6 μM. This high cytotoxicity is in line with the antiproliferative activity of this compound observed in an NCI60 screen (average GI_{50} ≈ 1 μM in a panel of 60 cancer cell lines upon 48-h treatment).[1]

[1] Accessed at https://dtp.cancer.gov/public_compare/ on 18/06/2021; compound identifier: NSC15300.

The cytotoxicity of all hybrids was found in the range between those of BG and acridine **8**. Thus, Bn-hybrids **7a–c** systematically demonstrated moderate cytotoxicity (15 μM < GI_{50} < 25 μM). Among N^9-hybrids, compound **19b** was also moderately cytotoxic (GI_{50} = 14.5 μM), while the analogues **19a** and **19c** showed high cytotoxicity (GI_{50} = 1.1 and 2.1 μM, respectively), approaching the value obtained for the acridine **8**. Finally, in the case of miscellaneous hybrids, the O^6-phenylguanine conjugate **13** was found to have high cytotoxic activity (GI_{50} = 0.8 μM), in the same range as its O^6-benzyl analogue **19a**, whereas the guanine conjugate **14** had no cytotoxic effects at concentrations lower than 25 μM. Considering the ensemble of the data obtained with these compounds, we can conclude that: (i) the cytotoxicity of BG derivatives is increased by conjugation of a 6-chloro-2-methoxyacridine moiety in hybrid compounds; (ii) as a general rule, N^9-hybrids are more cytotoxic than Bn-hybrids; and (iii) in the series of N^9-linked guanine–acridine hybrids, the nature of the substituent R in position 6 of the guanine moiety plays an important role in the molecule's cytotoxicity (**13** (R = Ph) > **19a** (R = Bn) > **14** (R = void)).

Cytotoxic effects of drugs in combination with TMZ: As a next step, the cytotoxic effects of the drugs were evaluated upon co-treatment with TMZ, aiming to determine the mutual effects of these combinations (additive, synergic or antagonistic). In these experiments, compounds were tested at single concentrations, representing either their GI_{50} values (Table 3) or 25 μM for compounds whose GI_{50} was higher than this value (BG and compounds **5**, **17a** and **18a**). TMZ was co-administrated at three concentrations (94, 188 and 375 μM), that correspond to 100%, 63%, and 50% viability at mono-treatment, respectively (cf. Figure S9). In drug combination experiments, compounds were added to cell cultures 2 h prior to addition of TMZ, following by incubation for 94 h in the presence of both drugs, which is a typical procedure for the assessment of MGMT inhibitors [11–13,38,56,60,61]. Bliss Independence model was used to analyze the combination effects of the drugs. This model assumes that the compounds acts independently, none of them interfering with the other drug's action but both contributing to the same outcome [62–64]. For the analysis in terms of this model, the experimental viability of cells treated by a combination of two drugs A and B ($V_{exp,AB}$) is compared with the theoretical viability of the combination calculated from the individual viability values obtained for the corresponding compounds ($V_{theo,AB} = V_A \times V_B$). The effect of a drug combination is interpreted as additive if the theoretical and experimental values match ($V_{exp} \approx V_{theo}$), synergic if $V_{exp} < V_{theo}$, and antagonistic if $V_{exp} > V_{theo}$ [62,63].

The results of combination experiments are presented in Figure 4 (for 94 μM TMZ) and Figure S10 (for 188 and 375 μM TMZ) and summarized in Table 4. BG was found to induce a clear synergic effect with TMZ used at a concentration of 94 μM, in agreement with what was observed in T98G and other MGMT-proficient cell lines [11,35,61]. BG derivatives **5**, **17a** and

18a also demonstrated synergy with TMZ in these conditions ($p < 0.0001$); these observations are in line with the previously documented ability of compound **5** to potentiate the activity of BCNU in the HT29 cell line [38]. Unexpectedly, acridine **8** also demonstrated strong synergy with subtoxic concentrations of TMZ. In case of the hybrids, none of the Bn-attached compounds were synergic, whereas among the N^9-hybrids, compounds **19a** and **19c** were synergic and compound **19b** probably as antagonist (cf. Figure 4 footnote). In the case of higher TMZ concentrations (188 or 375 µM), none of the BG derivatives devoid of the acridine moiety proved be synergic. At 188 µM TMZ, compounds **7a** and **7b** even showed an antagonist effect, while an additive effect was observed for all other compounds. Finally, at 375 µM TMZ, only compound **19a** and **19c** exhibited a synergic effect (Figure S10, Table 4).

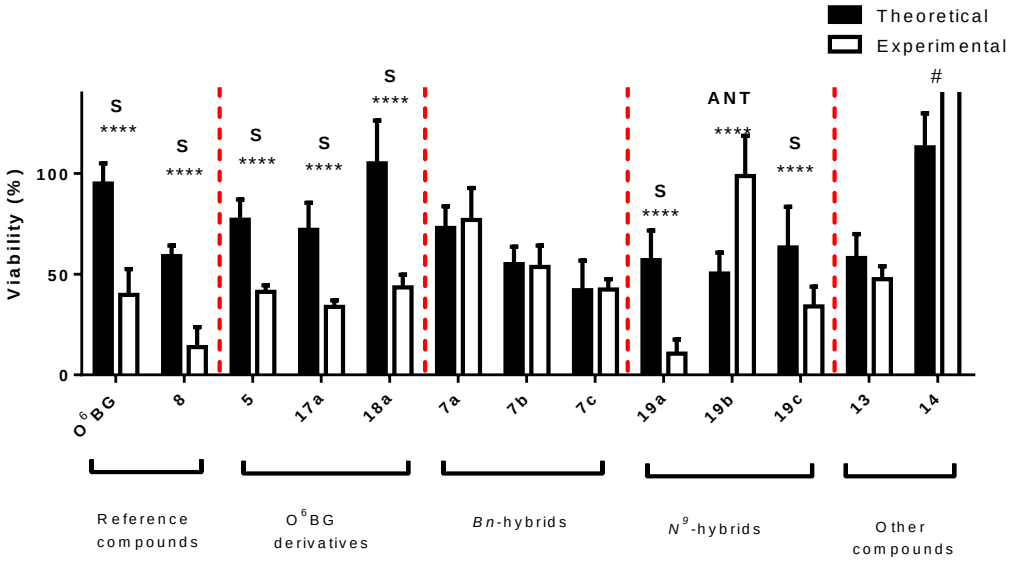

Figure 4. Bliss analysis of combinations of drugs (at their GI_{50} values, or 25 µM if $GI_{50} \geq 25$ µM) with TMZ (94 µM) in T98G cells. Black bars represent $V_{theo,AB}$ and its theoretical S.D. (see SI); white bars represent the experimental viability $V_{exp,AB}$ and its standard deviation from at least three biological replicates consisting of two technical replicates each. S and ANT stands for synergy or antagonism, respectively. One-way ANOVA with Sidak post-test comparison statistical analysis was performed; **** denote p values below 0.0001. [#] V > 150% was determined using CellTiter-Glo® kit; however, a cell counting experiment for this condition revealed a viability of ≥ 85%, indicating an interference with the CellTiter-Glo® kit. Therefore this result was not taken into account.

Table 4. Summary of combination effects of drugs with TMZ upon 96-h treatment in T98G cells.[a]

Compound	TMZ concentration (μM)		
	94	188	375
reference compounds			
acridine **8**	S (****)	A	ANT (***)
BG and derivatives			
BG	S (****)	A	A
5	S (****)	A	A
17a	S (****)	A	ANT (**)
18a	S (****)	A	A
Bn-hybrids			
7a	A	ANT (***)	A
7b	A	ANT (****)	ANT (****)
7c	A	A	ANT (*)
N^9-hybrids			
19a	S (****)	A	S (*)
19b	ANT (****)	ANT (**)	ANT (**)
19c	S (****)	A	S (*)
Other hybrids			
13	A	A	A
14	N/D[b]	A	A

[a] S, synergy, A, additive effect, ANT, antagonism; the asterisks indicate the *p*-level (*, **, *** and **** stand for *p* values ≤ 0.05, 0.01, 0.001 and 0.0001 respectively). [b] see # in Figure 4.

After screening the full panel of drugs, compounds **19a** and **19c** were studied in further detail along with BG control in a range of subtoxic doses (from ⅛ GI_{50} to GI_{50}) for both the drugs and TMZ (Figure S11). The viability data were analyzed by employing the Chou–Talalay method as implemented in the software CompuSyn [65,66]. In this method, the effect of the drug combination is represented by the value of Combination Index (CI), with CI > 1 being indicative of antagonist effect, CI < 1 of a synergic effect, and CI ≈ 1 of an additive effect, respectively. The results are represented as CI values as a function of the drug concentration, grouped by the employed TMZ concentrations (Figure 5).

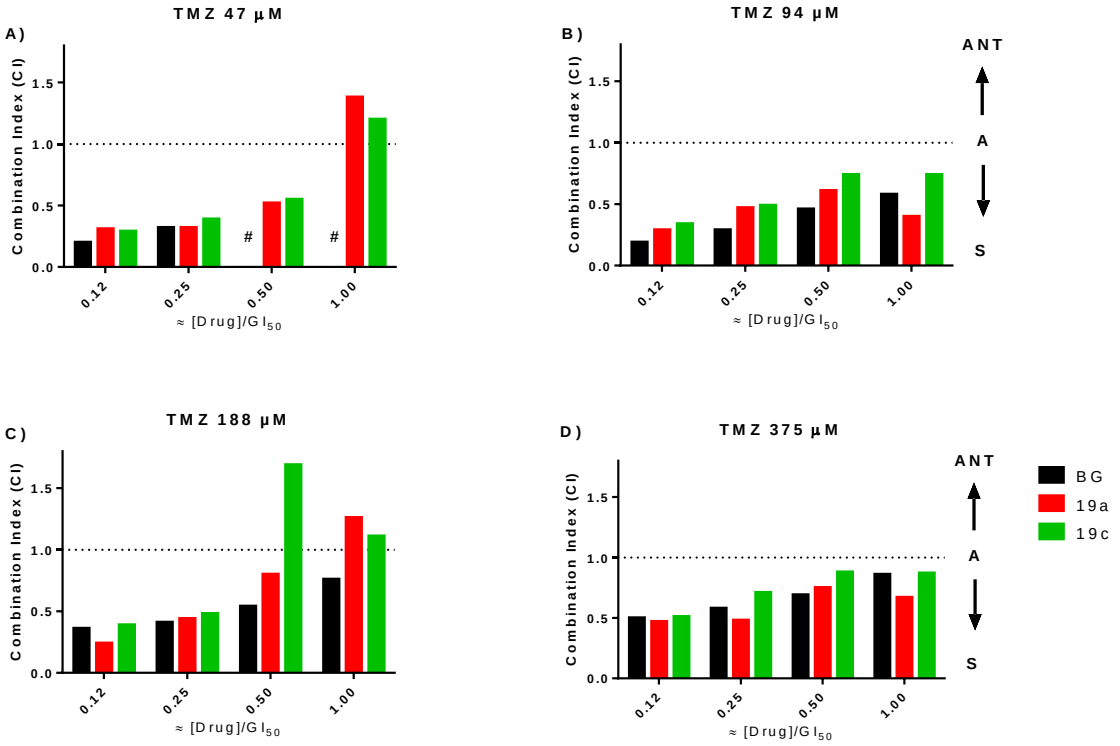

Figure 5. Combination Index (CI) values for combinations of drugs BG, **19a** and **19c** with TMZ in the range of concentrations from ⅛ GI_{50} to GI_{50} for each drug (GI_{50} = 92 µM for BG, 1.1 µM for **19a** and 2.1 µM for **19c**). #: these combinations were not analyzed due to an artifact similar to that observed in Figure 4, where the viability determined using CellTiter-Glo® kit was > 100% whereas viability by cell counting was ≈ 30%. Each CI value results from three biological replicates.

As a general trend, it can be observed that, for each TMZ concentration, CI values decrease and the synergy increases at low concentration of both drugs, reaching CI values as low as 0.2–0.3 at 47 µM TMZ and subtoxic (⅛ GI_{50}) concentration of the drugs. The comparison of CI values in Figure 5 shows that both hybrids are at least as efficient as BG in exerting synergy with TMZ in T98G cells, albeit at 40- to 80-fold lower concentration.

2.5. Microscopy studies

Due to fluorescent properties of the acridine moiety, the cellular localization of hybrids can be assessed by fluorescence microscopy. Towards this end, live-cell images of T98G cells were acquired after 96 h of incubation with compound **19a**. The green fluorescence of **19a** was observed in the cytosolic region (Figure 6, B) but not in the nucleus, as can be seen by DRAQ5

nuclear staining (Figure 6, A). It is also worth noting that the distribution of **19a** in the cytosol was not homogeneous; instead, the compound localized in the perinuclear region, as could be observed by the inspection of *Z*-stacked series of images (Figure S12).

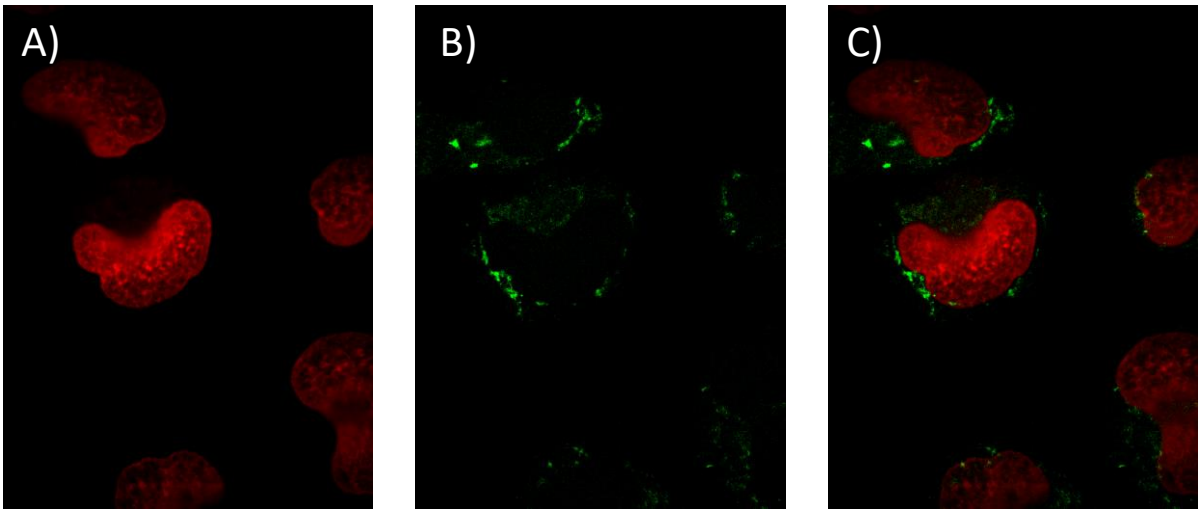

Figure 6. Representative in-plane confocal images of live T98G cells after 96 h of incubation in the presence of compound **19a** (1.1 µM). A) Fluorescence of DRAQ5 (642 / 700 nm channel); B) fluorescence of compound **19a** (488 / 525 nm channel); C) merged image.

2.6. Inactivation of cellular MGMT

In order to verify that treatment with the hybrid **19a** inactivates MGMT in live cells, we analyzed the residual activity of MGMT from cell extracts of T98G cells, following the treatment with compound **19a** or BG as a positive control (2 µM, 2 h) using the same coupled enzymatic assay (cf. Figure 3, A) [54,67]. The results (Figure 7) indicate that **19a** was indeed able to inactivate cellular MGMT in these conditions (by 50%), however less efficiently than BG (95% inhibition). These results demonstrate that, in agreement with its *in vitro* MGMT inhibition activity (cf. Figure 3), **19a** is also able to target MGMT in cells leading to its inactivation.

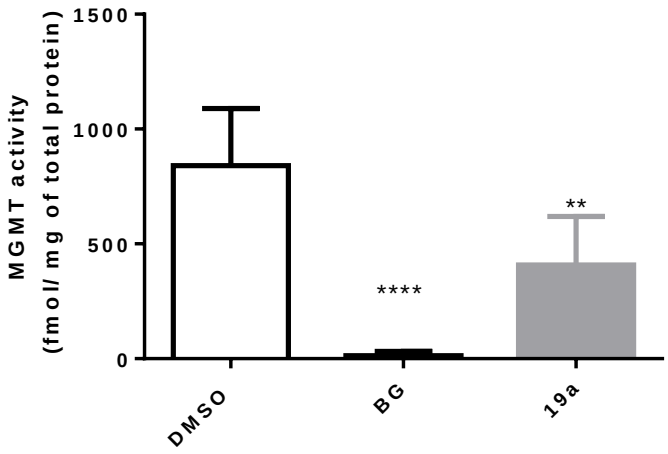

Figure 7. Inactivation of cellular MGMT activity in T98G cells treated for 2 h with compound **19a** (2µM), BG (2 µM), or DMSO as a vehicle. The MGMT activity determined by PAGE analysis was normalized to the total protein concentration in cellular extracts. Data are means ± s.d. from three biological replicates. One-way ANOVA; ****: $p \leq 0.0001$, **: $p \leq 0.01$.

2.7. DNA damage induction

To get insight into the mechanisms of cell death in the conditions of synergistic co-treatment with TMZ and **19a** (or BG as a control), we assessed the level of DNA double-strand breaks (DSB) in T98G cells through immunofluorescence assay using anti-γH2AX, a phosphorylated histone representing a well-established DSB marker [68]. Neither TMZ (94 µM) nor BG (92 µM) treatments induced significant change of the number or the size of γH2AX foci per nuclei; however, a combination of both induced a strong and statistically significant increase of the number (Figure 8) and size (Figures S13 and S14) of nuclear γH2AX foci, in agreement with the proposed mechanism of action of TMZ leading to DNA adducts followed by the accumulation of DSB resulting from the futile repair of O^6MeG residues [69–71]. Remarkably, neither compound **19a** (1.1 µM) nor its combination with TMZ induced an increase of the number or the size of γH2AX foci, despite a synergistic cytotoxic effect.

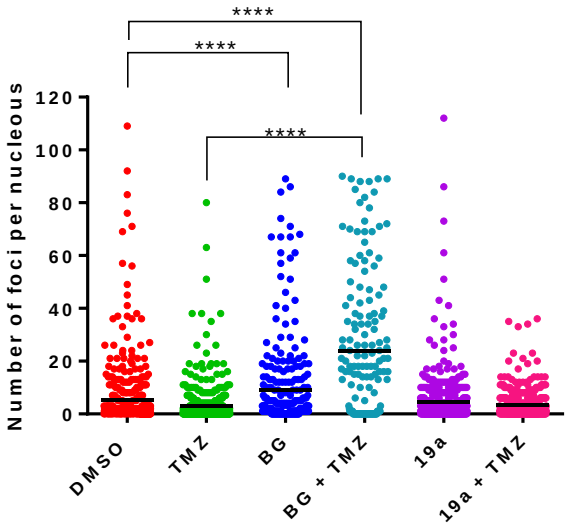

Figure 8. Impact of compounds on the number of nuclear γ-H2AX foci, as determined by immunostaining followed by fluorescence microscopy. Cells were incubated for 96 h with compound vehicle (DMSO 0.5% v/v), TMZ (94 µM), BG (92 µM), a combination of TMZ and BG (94 and 92 µM, respectively), compound **19a** (1.1 µM) and a combination of TMZ and **19a** (94 and 1.1 µM, respectively). Black bars indicate the mean values. At least 150 cells were counted per condition; data from two biological replicates. One-way ANOVA multi comparison with Tukey's post-test analysis; ****: $p \leq 0.0001$.

2.8. Apoptosis induction

In order to identify the mechanisms of cell death underlying the cytotoxic effects of the hybrids, we performed an Annexin V / propidium iodide (PI) cell death assay. Neither TMZ [72] nor BG treatments alone significantly increased the proportion of cells undergoing early apoptosis; however, their combination increased the fraction of apoptotic cells (from 2 to 8%) after 96 h, but not after 48 h (Figure 9, A), in agreement with literature [61] and in line with the DNA-damaging effects of this combination. Interestingly, compound **19a** alone significantly increased the fraction of early apoptotic cells (to 10%) after 96 h, but not after 48 h of treatment. The same effect was observed for a combination of **19a** with TMZ (11% after 96 h), indicating that the synergy of the cytotoxic effect of this combination does not stem from a synergistic apoptosis. In addition, no drug induced significant late apoptosis nor necrosis (Figure S15). Finally, to confirm that the compound **19a** triggers cell death by apoptosis, we assessed the activation of caspases using luminescent Caspase-Glo 3/7 assay. The results (Figure 9, B) clearly give evidence of activation of caspases in the cells treated with compound **19a** (1.4-fold with respect to DMSO control), which was not further increased in a combination of **19a** with TMZ.

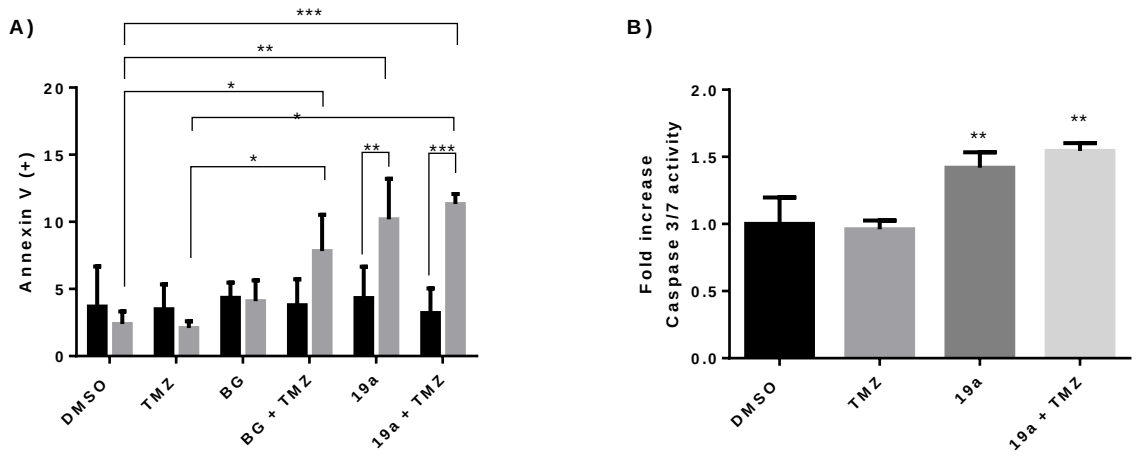

Figure 9. A) Results of the Annexin V / PI assay: fractions of early apoptosis in T98G cells after 48 h (black bars) and after 96 h (grey bars) of incubation with DMSO (0.5% v/v), TMZ (94 μM), BG (92 μM), a combination of TMZ (94 μM) and BG (92 μM), **19a** (1.1 μM), and a combination of TMZ (94 μM) and **19a** (1.1 μM), as determined by flow cytometry. Two-way ANOVA with a Tukey's multi comparison post-test. B) Caspase 3/7 activity of T98G cells treated for 96 h in the same conditions as described above. One-Way ANOVA test with a Dunnett's multi-comparison post-test; * ** and *** denote values of $p \leq 0.05$, 0.01, 0.001 respectively.

3. DISCUSSION

3.1. Intrinsic conformation, DNA binding, and *in vitro* MGMT inhibition by hybrid drugs

Photophysical properties of the hybrids give evidence that they adopt an intramolecular staked conformation in aqueous solutions, characterized by hypochromic and bathochromic effects on the acridine chromophore and a strong reduction of the fluorescence quantum yield, comparing with the reference acridine **8**. This conformation, stabilized by π-stacking interactions between the acridine and guanine units, is stable in a wide temperature range in aqueous solutions, but is disrupted in organic solvents. In this regard, the behavior of our acridine–BG hybrids is analogous to that of the conjugates of acridine with native nucleobases [49,50], with BG residue behaving as an efficient fluorescence quencher similar to guanine. While in the series of N^9-hybrids (**19a–c**) shorter linker resulted in more efficiently stacked hybrids (as estimated by the value of hypochromism *H*), in the series of Bn-hybrids **7a–c** the derivative with the shortest linker (**7a**) displayed the lowest hypochromism. This can be explained by a molecular model in which the benzyl group serving as the attachment point for

the two moieties stacks with the acridine ring, interfering – at least partially – with the stacking of the guanine residue (Figure S2).

Regardless the efficiency of intramolecular stacking, all hybrids were found to bind to double-stranded DNA with similar affinity (characterized by K_d values from 13 to 23 µM, Table 2), as indicated by photometric titrations, but without intercalation of the acridine moiety and thermal stabilization of the DNA duplex. This behavior is similar to that of structurally related intercalator–nucleobase conjugates that, despite their binding to double-stranded DNA evidenced by isothermal photometric titrations, do not lead to thermal stabilization of the undamaged duplex [73–75], and can be rationalized by a model where acridine–BG hybrids interact with DNA through external binding mode (Scheme 3, A). This is presumably due to the fact that energetic gain resulting from DNA intercalation by acridine is insufficient compensate for the penalty necessary to unfold the intramolecularly stacked ligand. Although the details of this DNA-binding mode are unknown, we can hypothesize that external binding to DNA leads to even stronger intramolecular stacking of hybrids, manifested by the increased hypochromic effect.

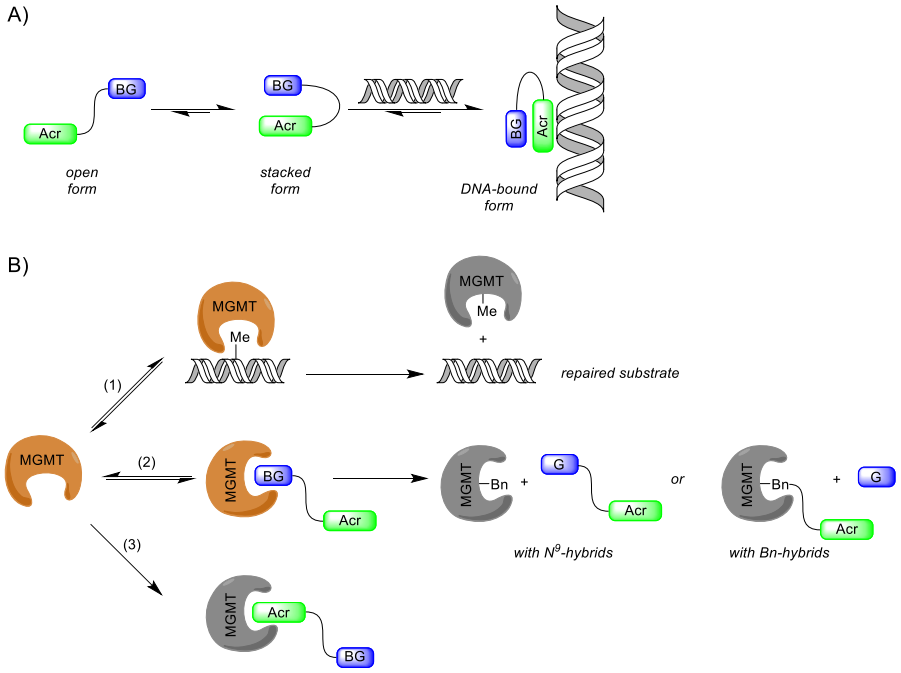

Scheme 3. Properties of BG–acridine hybrids. A) In the absence of DNA, the hybrids exist mainly in the intramolecular stacked form. Addition of ds DNA leads to external binding characterized by increased hypochromism of the acridine moiety. B) Inhibition of MGMT by BG–acridine hybrids. (1) Repair of the DNA substrate by MGMT; (2) inactivation of MGMT by BG–acridine hybrids through irreversible reaction of the BG moiety; (3) irreversible inhibition due to the acridine moiety. The inactivated MGMT is shown in gray.

The *in vitro* MGMT inhibition data revealed several complex patterns. In the standard conditions of this assay, the drug and the methylated DNA substrate compete for irreversible reaction with the enzyme (Scheme 3, B); as a result, the observed inhibitory effect stems from a combination of thermodynamic (i.e., the affinity of the drug to the active site of the enzyme) and kinetic (i.e., the velocity of reaction of the enzyme with the drug, relative to that of O^6MeG DNA substrate) effects. In addition, for DNA-binding inhibitors such as our hybrids, the presence of substrate or non-substrate DNA in the assay may play an additional role by sequestering the inhibitor, as evidenced by decreased inhibitory activity in the presence of CT DNA for most hybrids except compound **19c** (cf. Figure 3, B).

An interesting finding of our experiments was the fact that model acridine **8**, devoid of BG group, efficiently inhibited MGMT activity, with an inhibitory effect superior to that of BG in the conditions of the standard assay (Figure 3, B). One possible explanation of this finding would be a non-specific inhibitory effect due to sequestration of the DNA substrate in the intercalative complex. However, two facts speak against this hypothesis: (i) several well-known, strong DNA intercalators (ethidium bromide, daunomycin, doxycycline, and coralyne) did not inhibit MGMT in identical conditions (data not shown); (ii) the efficiency of MGMT inactivation by acridine **8** dramatically increased when this compound was pre-incubated with the enzyme, similarly to what was observed with BG (cf. Figure 3, B), whereas a mechanism based on a substrate-targeted inhibition (i.e., assuming that **8** interacts with the DNA, but not with the enzyme) would suggest identical activity in both setups. Altogether, these data indicate that acridine **8** inhibits the activity of MGMT, either through tight or irreversible binding or, eventually, due to aggregation effects leading to adsorption and loss of the enzyme. Interestingly, during the preparation of this manuscript, MGMT binding of structurally related acridone derivatives was suggested on the basis of molecular docking experiments [76]; moreover, inhibition of MGMT activity by other polyaromatic compounds was previously documented [77]. Inactivation of MGMT by the acridine residue can also explain the inhibitory effect of the hybrids **13** and **14** that do not contain a BG moiety, as well as an increase of the inhibitory activity of all hybrids observed upon pre-incubations of compounds with the enzyme prior to addition of the target. While the extensive studies of MGMT inhibition by acridine and its derivatives are outside the scope of this work, it is clear that the properties of BG–acridine hybrids are strongly influenced by the acridine moiety that, on one hand, modulates the properties of the BG counterpart (by stacking interactions and by interaction with DNA, see Scheme 3) and, on the other hand, interacts with the enzyme itself, at least in the case of compound **8**.

3.2. Antiproliferative activity, synergy with TMZ and cell death mechanisms

Similarly to *in vitro* properties, the molecular design of hybrids has an influence on their cytotoxic effects, as illustrated by the fact that the activity of all hybrids falls in the range between that of weakly cytotoxic BG and the highly cytotoxic acridine **8**. However, while all hybrids inhibited – to a varied extent – MGMT activity *in vitro*, only N^9-hybrids **19a** and **19c** exerted drug synergy upon co-treatment with TMZ in MGMT-expressing T98G cells. For both **19a** and **19c**, as well as for BG, the magnitude of synergy effect, quantitatively expressed through CI values, was stronger at low concentrations of both TMZ and MGMT inhibitors (cf. Figure 5). The lack of synergy at higher doses of TMZ and/or inhibitors may be due to the "cytotoxicity burst" effect, i.e., activation of multiple stress responses, in near-cytotoxic conditions, in contrast to sub-toxic conditions where the cell death is due to one predominant mechanism, i.e. O^6MeG-induced toxicity [78]. While the synergy with TMZ and inactivation of cellular MGMT (cf. Figure 7) may suggest that cellular effects of **19a** are similar to BG, the mechanism underlying this synergy appears to be quite different. Indeed, while the combination of BG with TMZ strongly increased the number of DSB and the fraction of cells undergoing apoptosis, neither **19a** alone nor in combination with TMZ did not show any DSB increase; however, both treatments induce apoptosis at the same level (cf. Figures 8 and 9). This gives evidence that cytotoxic mechanisms of this hybrid (and its combination with TMZ) are more complex: in the case of combination of BG with TMZ, the apoptosis clearly seems to stem from the DNA damage. In contrast, the combinations of **19a** with TMZ leads to synergy effect on the cytotoxicity level independently of DNA damage or increased apoptosis. This is plausible since TMZ may sensitize also glioblastoma cell lines via other pathways than DNA damage (such as autophagy) [79]. Moreover, the apoptotic effect of compound **19a** may be attributed to the presence of acridine fragment that is able to activate many signaling cascades, as described for related 9-aminoacridine derivatives [22,23].

Despite the presence of a DNA-interacting acridine moiety, compound **19a** was found to localize in perinuclear region of the cytoplasm; indeed, its presence in the nucleus of live cells could not be detected by confocal microscopy even upon long incubation time (96 h). This finding is rather unexpected, as structurally similar acridine–melamine hybrids were shown adopt strictly nuclear localization [31]; however, they it can be rationalized taking into account the absence of intercalative DNA binding by the hybrids. Moreover, similar peri-nuclear localization was observed for acridine dimers [80]. As MGMT is known to adopt both nuclear and cytosolic localization [81,82], the absence of nuclear staining by **19a** is consistent with inactivation of cellular MGMT; however, it may also point to a different mechanism. Of note, the observed fluorescence may arise from the product of enzymatic debenzylation of **19a** (i.e., compound **14**) accumulating, e.g., in transport vesicles.

Remarkably, acridine **8** itself also demonstrated strong synergy effect with low doses of TMZ. This effect is in line with the recently described activity of structurally related acridones to potentiate the cytotoxic effects of TMZ [76]. While the detailed studies of the mechanism of intrinsic cytotoxic effects of this compound are outside the scope of this work, this unexpected property represents a novel addition to a multitude of biological effects of acridine derivatives.

From the practical point of view, the capacity of BG–acridine hybrids to inhibit the growth of a multidrug-resistant glioblastoma cell line alone or in combination with sub-toxic doses of TMZ represents significant interest. To address the potential of therapeutic use for these compounds, we performed *in silico* evaluation of their physicochemical and ADME parameters and drug-likeness, including the potential to cross the BBB [83]. The results (Table S1) demonstrate that, in contrast to BG and acridine **8**, most hybrids can be seen as rather poor drug candidates according to the classical criteria of medicinal chemistry, with only **19a** and **19b** satisfying the Lipinski filter. However, the evaluation of BBB permeability using AlzPlatform database [84] indicates that most hybrids are potentially able to cross the BBB and reach brain tumors. It should be noted that brain tumors are known to compromise the BBB integrity, resulting in a vasculature known as the blood–tumor barrier (BTB), which is highly heterogeneous and characterized by non-uniform permeability, rendering its *in silico* prediction rather challenging [85,86].

4. CONCLUSIONS

In this work, we designed, synthesized and studies two panels of hybrid compounds, combining a DNA-intercalating 9-amino-6-chloro-2-methoxyacridine moiety with O^6-benzyl-guanine unit capable of deactivation of MGMT. We demonstrated that all hybrids were able to (i) interact with DNA, presumably through external binding, and (ii) inactivate MGMT *in vitro* with varied efficiency, depending on the chemical structure of the hybrid, the presence of non-substrate DNA, and the conditions of the experimental setup, revealing the mutual influence of both constituents on the DNA-binding and enzyme-inhibiting properties. Importantly, hybrid **19a** was also able to inactivate MGMT in cells. All hybrids displayed moderate cytotoxicity in TMZ-resistant glioblastoma cells; however, only two N^9-hybrids, **19a** and **19c**, displayed pronounced synergy effect with DNA-alkylating prodrug TMZ in sub-cytotoxic conditions. Our findings clearly suggest that compound **19a** induces cell death alone and in synergy with TMZ through a different pathway than BG. While the detailed studies of these effects are outside the scope of this work, the antiproliferative properties of this new series of hybrids may potentially be exploited in a strategy to treat cells resistant to the BG / TMZ combination and represent a novel addition to the panel of biological activities of acridines.

5. EXPERIMENTAL SECTION

5.1. Chemistry

General remarks: All commercially available chemicals were reagent grade and used without further purification. NMR spectra were measured with a Bruker Avance 300 spectrometer at 25 °C; chemical shifts are given in ppm (δ) values. Multiplicities of ^{13}C NMR signals were determined from DEPT-135 or APT experiments. The purity of final compounds was assessed by LC/MS analysis (Waters Alliance 2525 equipped with a Phenomenex Luna Omega 3 µm Polar C_{18} 100A column and Waters 2996 photodiode array detector; eluent A: water with 0.1% HCOOH, eluent B: MeCN with 0.1% HCOOH, gradient elution with 2 to 100% of eluent B). Mass spectra were obtained on a Waters ZQ spectrometer using electrospray ionization (ESI). HRMS analysis were performed at the Small Molecule Mass Spectrometry platform of ICSN (Centre de Recherche de Gif Sur Yvette, France).

(3-(Aminomethyl)phenyl)methanol (1) [38]: In a two-neck round flask under an Ar atmosphere, 3-cyanobenzoic acid (10.0 g, 67.9 mmol) was suspended in anhydrous THF (50 mL) while cooling at 0 °C. THF·BH_3 complex (1 M in THF, 200 mL, 200 mmol) was added dropwise and the reaction was stirred for 24 h at room temperature. The mixture was quenched with a mixture of concentrated HCl (37%) and H_2O (1:1, 100 mL). THF was removed under vacuum and NaOH pellets were carefully added until pH 12 was reached. The aqueous phase was extracted with Et_2O (11 × 200 mL); the organic layers were dried over Na_2SO_4, filtered and concentrated under vacuum. The amino alcohol **1** (9.1 g, 66.3 mmol, 98%) was obtained as a white solid and immediately stored under Ar at –20 °C. ^1H NMR ($CDCl_3$, 300 MHz): δ 2.45 (s, 3H), 3.77 (s, 2H), 4.59 (s, 2H), 7.14–7.31 (m, 4H).

***N*-(3-(Hydroxymethyl)benzyl)trifluoroacetamide (2)** [38]: Amino alcohol **1** (885 mg, 6.45 mmol) was dissolved in 10 mL of dry MeOH under an Ar atmosphere. Triethylamine (896 µL, 650 mg, 6.45 mmol) was added, the reaction mixture was cooled to 0 °C, and ethyl trifluoroacetate (998 µL, 1.187 g, 8.38 mmol) was added dropwise. The reaction mixture was allowed to return to room temperature while stirring for 1 h. After removal of MeOH in vacuum, the crude product was dissolved in AcOEt (10 mL) and washed with H_2O (10 mL). The aqueous layer was extracted with AcOEt (3 × 20 mL), the organic layers were pooled, dried over Na_2SO_4, filtrated and concentrated under vacuum. The product was purified by flash chromatography (SiO_2, eluent: cyclohexane / AcOEt, 2:1; R_f = 0.25), to give **2** (1.00 g, 4.28 mmol, 66%) as a white solid. ^1H NMR ($CDCl_3$, 300 MHz): δ 1.93 (s, 1H), 4.53 (d, J = 5.7 Hz, 2H), 4.69 (s, 2H), 6.69 (s, 1H), 7.21–7.40 (m, 4H); ^{13}C NMR, ($CDCl_3$, 75 MHz): δ 43.9 (CH_2), 64.9 (CH_2), 118.0 (C_q, J = 287 Hz), 126.5 (CH), 126.9 (CH), 127.2 (CH), 129.3 (CH), 136.1

(C_q), 141.8 (C_q), 157.1 (C_q), 157.2 (C_q); MS (ESI^+): *m*/*z* (%) 257.1 (5) [*M* + Na]$^+$, 216.2 (100) [*M* – OH]$^+$.

1-(2-Amino-9*H*-purin-6-yl)-1-methylpyrrolidin-1-ium chloride (3) [38]: Under an Ar atmosphere, 2-amino-6-chlorpurine (1.00 g, 5.89 mmol) was suspended in dry DMF (30 mL) and heated for 2 h at 50 °C to dissolve the reagent. Upon cooling to room temperature, 1-methylpyrrolidine (1.4 mL, 1.15 g, 13.50 mmol) was added and the mixture was stirred for 18 h. Then, cold acetone (2 mL) was added and the precipitate was collected by filtration, washed with Et_2O (2 × 20 mL) and dried in vacuum to obtain **3** (791 mg, 3.10 mmol, 53%) as a white solid. ^{1}H NMR (DMSO-d_6, 300 MHz): δ 2.05 (m, 2H), 2.12 (m, 2H), 3.65 (s, 3H), 3.98 (m, 2H), 4.60 (m, 2H), 7.12 (s, 2H), 8.35 (s, 1H), 13.48 (br s, 1H); ^{13}C NMR (DMSO-d_6, 75 MHz): δ 21.4 (CH_2), 51.5 (CH_3), 64.0 (CH_2), 116.0 (C_q), 142.9 (CH),151.6 (C_q),158.6 (C_q), 159.0 (C_q); MS (ESI^+) *m*/*z* (%) 219.2 (100) [*M* – Cl]$^+$.

***N*-(3-(((2-amino-9*H*-purin-6-yl)oxy)methyl)benzyl)-2,2,2-trifluoroacetamide (4)** [38]: Under an Ar atmosphere, alcohol **2** (415 mg, 1.78 mmol) was dissolved in dry DMF (5 mL) together with *t*-BuOK (1.02 g, 9.14 mmol) and the mixture was stirred for 30 min at room temperature, followed by the addition of salt **3** (228 mg, 0.89 mmol). The mixture was stirred for 5 h at room temperature. The solvent was removed under vacuum and the crude mixture was purified by flash chromatography (SiO_2, eluent: DCM / EtOH, 95:5 to 90:10) to yield **4** (304 mg, 0.82 mmol, 47%) as a white solid. ^{1}H NMR (DMSO-d_6, 300 MHz): δ 4.41 (d, *J* = 5.8 Hz, 2H), 5.48 (s, 2H), 6.29 (s, 2H), 7.24–7.42 (m, 4H), 7.81 (s, 1H), 10.03 (t, *J* = 5.8 Hz, 1H), 12.42 (s, 1H); MS (ESI^+): *m*/*z* (%) 367.1 (100) [*M* + H]$^+$.

6-((3-(Aminomethyl)benzyl)oxy)-9*H*-purin-2-amine (5) [38]. **Method A:** In a mixture of MeOH (26 mL) and H_2O (800 µL), compound **4** (366 mg, 0.72 mmol) and K_2CO_3 (500 mg, 3.6 mmol) were resuspended and the mixture was refluxed for 4 h until the disappearance of the starting material (TLC). The solvent was removed and the crude product was purified by flash chromatography (SiO_2, eluent: DCM / MeOH / TEA, 80:20:1, R_f = 0.2) to give **5** (108 mg, 0.39 mmol, 55%) as a white solid. ^{1}H NMR (DMSO-d_6, 300 MHz): δ 3.74 (s, 2H), 5.46 (s, 2H), 6.28 (s, 2H), 7.31–7.33 (m, 3H), 7.47 (s, 1H), 7.83 (s, 1H); ^{13}C NMR (DMSO-d_6, 75 MHz): δ 45.4 (CH_2), 66.9 (CH_2), 126.5 (CH), 126.8 (CH), 127.3 (CH), 128.2 (CH), 136.4 (C_q), 138.2 (CH), 144.0 (C_q), 159.5 (C_q); MS (ESI^+): *m*/z (%) 271.2 (100) [*M* + H]$^+$. **Method B:** In an Ar atmosphere, compound **2** (2.19 g, 9.39 mmol) was dissolved in dry pyridine (30 mL) and *t*-BuOK (2.12 g, 18.93 mmol) were added. The reaction mixture was stirred for 20–30 min at room temperature, followed by the addition of salt **3** (1.20 g, 4.71 mmol). After 6 h, more *t*-BuOK (2.12 g, 18.93 mmol) was added and the reaction was stirred overnight. Then, **2** (2.19 g, 2.39 mmol) was added to the mixture, which was finally stirred for 24 h more. Finally, H_2O

(6 mL) was added and the mixture was refluxed for 2 h. The solvents were removed under vacuum and the crude purified as described above to yield **5** (1.03 g, 3.80 mmol, 81%); the spectroscopic data were identical with those given above.

3-((6-Chloro-2-methoxyacridin-9-yl)amino)propanoic acid (6a) [46]: In a two-neck flask, 6,9-dichloro-2-methoxyacridine (1.00 g, 3.59 mmol) was mixed with PhOH (4.00 g, 42.5 mmol) and β-alanine (247 mg, 3.89 mmol), and the reaction was heated for 3 h at 110 °C. The dark-brown solution was cooled to room temperature an Et_2O (20 mL) was added. The precipitated yellow solid was collected by filtration, dissolved in aq. NaOH (1 M, 100 mL), and filtered. The filtrate was acidified to pH 7. The yellow precipitate was collected, washed with H_2O (2 × 20 mL), MeOH (1 × 10 mL) and Et_2O (2 × 30 mL), and dried over P_2O_5 to yield **6a** (1.05 g, 3.17 mmol, 89%) as a yellow solid. ^{1}H NMR (DMSO-d_6, 300 MHz): δ 3.93–3.98 (m, 5H), 7.29 (dd, *J* = 9.2 Hz, 2.0 Hz, 1H), 7.40 (dd, *J* = 9.3, 2.4 Hz, 1H), 7.66 (d, *J* = 9.3 Hz, 1H), 7.81–7.85 (m, 2H), 8.36 (d, *J* = 9.2 Hz, 1H); ^{13}C NMR (DMSO-d_6, 75 MHz): δ 36.5 (CH_2), 46.5 (CH_2), 55.5 (CH_3), 100.9 (CH), 114.8 (C_q), 117.3 (C_q), 119.2 (C_q), 122.2 (CH), 124.1 (CH), 126.6 (CH), 130.1 (CH), 133.3 (CH), 145.6 (C_q), 147.9 (C_q),150.5 (C_q), 155.5 (C_q), 174.4 (C_q); MS (ESI$^+$): *m*/*z* (%) 331.2 (100) [*M* + H]$^+$.

2-(2-(2-((6-Chloro-2-methoxyacridin-9-yl)amino)ethoxy)ethoxy)acetic acid (6b): Under an Ar atmosphere, 6,9-dichloro-2-methoxyacridine (300 mg, 1.07 mmol) was mixed with PhOH (3.00 g, 31.8 mmol) and the mixture was heated at 70 °C for 1 h. Then, 2-[2-(2-aminoethoxy)ethoxy]acetic acid (194 mg, 1.18 mmol) was added and the temperature was increased to 110 °C for 3 h. The reaction mixture was cooled to room temperature, filtrated, and the solid washed with Et_2O (2 x 30 mL) and purified by flash chromatography (SiO_2, eluent: DCM / MeOH / TEA, 95:5:1, R_f = 0.26) to yield **6b** (426 mg, 1.05 mmol, 98%) as a yellow powder. ^{1}H NMR (DMSO-d_6, 300 MHz): δ 3.55 (s, 4H), 3.71 (t, *J* = 5.2 Hz, 2H), 3.86 (t, *J* = 5.2 Hz, 2H), 3.933.95 (m, 5H), 7.34 (dd, *J* = 9.2, 2.1 Hz, 1H), 7.44 (dd, *J* = 9.4, 2.4 Hz, 1H), 7.64 (d, *J* = 2.4 Hz, 1H), 7.83 (d, *J* = 9.4 Hz, 1H), 7.88 (d, *J* = 2.1 Hz, 1H), 8.38 (d, *J* = 9.2 Hz, 1H); ^{13}C NMR (APT, DMSO-d_6, 75 MHz, 40 °C): δ 49.2 (CH_2), 55.5 (CH_3), 67.6 (CH_2), 69.6 (CH), 69.7 (CH), 69.9 (CH), 101.1 (CH), 115.1 (C_q), 117.6 (C_q), 122.8 (C_q), 124.1 (CH),126.1 (CH), 126.4 (CH), 129.6 (C_q), 133.6 (C_q), 145.1 (C_q), 147.1 (C_q), 147.3 (C_q), 150.6 (C_q), 155.1 (C_q), 171.4 (C_q); MS (ESI$^+$): *m*/*z* (%) 405.2 (100) [*M* + H]$^+$.

8-((6-Chloro-2-methoxyacridin-9-yl)amino)octanoic acid (6c): 6,9-dichloro-2-methoxy-acridine (300 mg, 1.07 mmol) was mixed with PhOH (3.00 g, 31.8 mmol) under an Ar atmosphere and the mixture was heated at 70 °C for a period of 1 h. Then, 8-aminocaprylic acid (189 mg, 1.18 mmol) was added and the temperature was increased to 110 °C for 3 h. The reaction mixture was cooled to room temperature, filtrated, the solid was washed with

Et_2O (2 × 30 mL) and purified by flash chromatography (SiO_2, eluent: DCM / MeOH / TEA, 95:5:1, R_f = 0.20). Compound **6c** (405 mg, 1.01 mmol, 94%) was obtained a yellow solid. ^{1}H NMR (DMSO-d_6, 300 MHz): δ 1.42–1.49 (m, 6H), 1.51 (dt, *J* = 7.5, 6.9 Hz, 2H), 1.85 (dt, *J* = 8.1, 6.3 Hz, 2H), 2.15 (t, *J* = 7.2 Hz, 2H), 3.96 (s, 3H), 4.03 (t, *J* = 6.9 Hz, 2H), 7.48 (dd, *J* = 9.2, 1.9 Hz, 1H), 7.65 (dd, *J* = 9.3, 2.3 Hz, 1H), 7.88 (d, *J* = 9.3 Hz, 1H), 7.95 (m, 2H), 8.5 (d, *J* = 9.2 Hz, 1H), 9.56 (s, 1H), 12.0 (s, 1H); ^{13}C NMR (APT, DMSO-d_6, 75 MHz): δ 24.8 (CH_2), 26.5 (CH_2), 28.8 (CH_2, 2C), 29.5 (CH_2), 34.1 (CH_2), 49.2 (CH_2), 56.6 (CH_3), 104. 1 (CH), 110.9 (C_q), 114.9 (C_q), 118.6 (C_q), 121.8 (CH), 123.6 (CH), 127.2 (CH), 127.6 (CH), 129.1 (CH), 138.8 (C_q), 155.9 (C_q), 156.2 (C_q), 174.9 (C_q); MS (ESI$^+$): *m*/*z* (%) 401.3 (100) [*M* + H]$^+$.

***N*-(3-(((2-amino-9*H*-purin-6-yl)oxy)methyl)benzyl)-3-((6-chloro-2-methoxyacridin-9-yl)amino)propanamide (7a):** Compound **6** (159 mg, 0.48 mmol) was dissolved in dry DMF (10 mL) under an Ar atmosphere together with DIPEA (249 µL, 195 mg, 1.51 mmol), HBTU (364 mg, 0.96 mmol), and HOBt (13 mg, 0.09 mmol). The mixture was stirred for 30 minutes and then **5** (143 mg, 0.52 mmol) was added to the mixture. The reaction mixture was stirred for 24 h at room temperature, then H_2O (10 mL) was added and the crude mixture was extracted with a mixture of DCM and MeOH (9:1, 4 × 50 mL). The organic layers were pooled, dried over Na_2SO_4, filtrated and concentrated under vacuum. The reaction was purified two times by flash chromatography (SiO_2, eluent: DCM / MeOH / TEA, 95:5:1, R_f = 0.12) to yield **7a** (76 mg, 0.13 mmol, 27%) as a yellow solid. ^{1}H NMR (DMSO-d_6, 300 MHz, 40 °C): δ 1.24 (s, 1H), 2.64 (m, 2H), 3.91 (s, 3H), 4.05 (m, 2H), 4.26 (m, 2H), 5.42 (s, 2H), 9.18 (s, 2H), 7.15–7.45 (m, 6H), 7.80–7.86 (4H), 8.37–8.44 (m, 2H), 12.36 (br s, 1H); ^{13}C NMR (APT, DMSO-d_6, 75 MHz, 40 °C): δ 35.9 (CH_2), 41.9 (CH_2), 45.9 (CH_2), 55.5 (CH_3), 66.5 (CH_2), 101.4 (CH), 109.7 (CH), 114.4 (C_q), 117.1 (CH), 118.8 (CH), 122.8 (CH), 123.9 (CH), 124.4 (CH), 126.7 (CH), 126.8 (CH), 127.1 (CH), 128.2 (CH), 134.8 (C_q), 136.6 (C_q), 139.4 (C_q), 144.2 (C_q, observed by HMBC), 146.3 (C_q), 150.9 (C_q), 155.1 (2C, C_q), 159.5 (C_q), 170.3 (C_q); MS (ESI$^+$): *m*/*z* (%) 583.3 (10) [*M* + H]$^+$, 292.2 (100) [*M* + 2H]$^{2+}$; purity (HPLC): 97%; HRMS (TOF ESI$^+$): calcd. for $C_{30}H_{28}ClN_8O_3$ [*M* + H]$^+$: 583.1973, found: 583.1993.

***N*-(3-(((2-amino-9*H*-purin-6-yl)oxy)methyl)benzyl)-8-((6-chloro-2-methoxyacridin-9-yl)-amino)octanamide (7b):** Compound **8** (80 mg, 0.19 mmol) was dissolved in dry DMF (8 mL) under an Ar atmosphere together with DIPEA (98 µL, 77 mg, 0.59 mmol), HBTU (90 mg, 0.23 mmol), and HOBt (5 mg, 0.04 mmol). The mixture was stirred for 30 min and then **5** (80 mg, 0.29 mmol) was added. The reaction was stirred for 24 h at room temperature. After addition of H_2O (10 mL), the crude was extracted with a mixture of DCM and MeOH (9:1, 5 × 50 mL). The organic layers were pooled, washed with H_2O and brine (1× 30 mL each), dried over Na_2SO_4, filtered and concentrated in vacuum. The residue was purified two times by flash chromatography (SiO_2, eluent: DCM / MEOH / TEA, 95:5:1, R_f = 0.14). Compound **7b** (85 mg,

0.12 mmol, 65%) was obtained as a yellow solid. ^{1}H NMR ($MeOD_4$, 300 MHz): δ 3.64 (s, 4H), 3.77 (t, *J* = 5.1 Hz, 2H), 3.89 (s, 3H), 3.96–3.97 (m, 5H), 4.21 (s, 2H), 5.28 (s, 2H), 7.02 (d, *J* = 7.4 Hz, 1H), 7.12 (t, *J* = 7.5 Hz, 1H), 7.19 (d, *J* = 7.4 H, 1H), 7.24–7.29 (m, 2H), 7.45 (d, *J* = 9.3 Hz, 1H), 7.55 (m, 1H), 7.70-7.73 (m, 2H), 7.80 (s, 1H), 8.26 (d, *J* = 9.3 Hz, 1H). ^{13}C NMR (APT, $MeOD_4$, 75 MHz): δ 43.2 (CH_2), 49.6 (CH_2), 56.4 (CH_3), 68.6 (CH_2), 70.8 (CH_2), 71.1 (CH_2), 71.2 (2C, CH_2), 72.0 (CH_2), 102.5 (CH), 114.4 (C_q), 117.5 (C_q), 123.3 (CH), 124.9 (CH), 126.5 (CH), 127.3 (CH), 127.8 (CH), 128.0 (CH), 128.1 (CH), 129.6 (CH), 138.0 (C_q), 138.8 (C_q), 139.7 (C_q), 139.9 (CH), 142.2 (C_q), 145.5 (C_q), 155.3 (C_q), 157.6 (C_q), 161.2 (C_q), 161.6 (C_q), 172.5 (C_q); MS (ESI$^+$): *m*/*z* (%) 657.4 (5) $[M + H]^+$, 329.3 (100) $[M + 2H]^{2+}$; purity (HPLC): 97%; HRMS (TOF ESI$^+$): calcd. for $C_{33}H_{34}ClN_8O_5$ $[M + H]^+$: 657.2335, found: 657.2364.

***N*-(3-(((2-amino-9*H*-purin-6-yl)oxy)methyl)benzyl)-8-((6-chloro-2-methoxyacridin-9-yl)-amino)octanamide (7c):** Compound **10** (100 mg, 0.25 mmol) was dissolved in dry DMF (10 mL) under an Ar atmosphere together with DIPEA (124 µL, 97 mg, 0.75 mmol), HBTU (114 mg, 0.30 mmol) and HOBT (7 mg, 0.05 mmol). The mixture was stirred for 30 min and **5** (101 mg, 0.38 mmol) was added. The reaction was stirred for 24 h at room temperature. After addition of H_2O (10 mL), the crude was extracted with a mixture of DCM / MeOH (9:1, 5 × 50 mL). The organic layers were pooled, washed with H_2O and brine (1 × 30 mL each), dried over Na_2SO_4, filtrated and concentrated under vacuum. The product was purified two times by flash chromatography (SiO_2, eluent: DCM / MeOH / TEA, 95:5:1, R_f = 0.12) to yield compound **7c** (106 mg, 0.16 mmol, 65%) as a yellow solid. ^{1}H NMR ($MeOD_4$, 300 MHz): δ 1.27–1.31 (m, 8H), 1.52–1.57 (m, 2H), 1.72–1.77 (m, 2H), 2.16 (t, *J* = 7.3 Hz, 2H), 3.80 (t, *J* = 7.2 Hz, 2H), 3.93 (s, 3H), 4.34 (s, 2H), 5.46 (s, 2H), 7.19–7.44 (m, 6H), 7.53 (d, *J* = 2.6 Hz, 1H), 7.77–7.82 (m, 3H), 8.24 (d, *J* = 9.4 Hz, 1H); ^{13}C NMR (APT, $MeOD_4$, 75 MHz): δ 25.3 (CH_2), 26.3 (CH_2), 28.5 (CH_2), 30.5 (CH_2), 35.5 (CH_2), 42.5 (CH_2), 49.5 (CH_2), 54.9 (CH_3), 67.4 (CH_2), 100.1 (CH), 113.9 (C_q), 116.6 (C_q), 122.9 (CH), 125.0 (CH), 126.7 (CH, 2C), 126.9 (CH, 2C), 127.0 (CH), 128.2 (CH), 135.6 (C_q), 136.7 (C_q), 138.6 (CH), 139.1 (C_q), 152.3 (C_q), 155.9 (C_q), 172.1 (C_q), 174.5 (C_q); MS (ESI$^+$): *m*/*z* (%) 653.5 (5) $[M + H]^+$, 327.4 (100) $[M + 2H]^{2+}$; purity (HPLC): 97%; HRMS (TOF ESI$^+$): calcd. for $C_{35}H_{38}ClN_8O_3$ $[M + H]^+$: 653.2570, found: 657.2782.

6-Chloro-2-methoxyacridin-9-amine (28):[27,87] 6,9-dichloro-2-methoxyacridine (1.00 g, 3.59 mmol) was mixed with PhOH (3.00 g, 31.80 mmol) under an Ar atmosphere and the reaction was heated at 70 °C for a period of 1 h. Then, $(NH_4)_2CO_3$ (700 mg, 7.28 mmol) was added and the temperature was increased to 110 °C for 3 h. The reaction was cooled, the solid was collected by filtration, washed with 10% aq. NaOH (3 × 20 mL), H_2O (2 × 20 mL), DCM (2 × 10 mL), acetone (1 × 10 mL) and then dried over P_2O_5 to yield compound **8** (750 mg, 2.89 mmol, 81%) as a yellow solid. ^{1}H NMR (DMSO-d_6, 300 MHz): δ 3.91 (s, 3H), 7.30 (dd, *J* = 9.2, 1.3 Hz, 1H), 7.37 (dd, *J* = 9.3, 1.9 Hz, 1H), 7.67 (d, *J* = 1.9 Hz, 1H), 7.70 (s, 2H),

7.80 (d, *J* = 1.3 Hz, 1H), 8.30 (d, *J* = 9.2 Hz, 1H); ^{13}C NMR (DMSO-d_6, 75 MHz): δ 55.7 (CH_3), 100.3 (CH), 111.2 (C_q), 113.2 (C_q), 122.0 (CH), 124.4 (CH), 125.3 (CH), 126.9 (CH), 130.5 (CH), 133.6 (C_q), 145.9 (C_q), 147.7 (C_q), 148.7 (C_q), 154.6 (C_q); MS (ESI$^+$): *m/z* (%) 259.0 (100) [*M* + H]$^+$, purity (HPLC): 98%.

***tert*-Butyl (4-bromobutyl)carbamate (9)**:[88] Under an Ar atmosphere, 500 mg (2.02 mmol) of 4-bromobutan-1-amine hydrobromide (500 mg, 2.02 mmol) was dissolved in dry THF (10 mL) at 0 °C together with $(Boc)_2O$ (519 mg, 2.37 mmol) and triethylamine (360 µL, 262 mg, 2.59 mmol). After reaching room temperature, the mixture was stirred for 24 h. The solvent was removed under vacuum and the sample diluted DCM (50 mL). The organic layer was washed with 5% aq. HCl (15 mL) and H_2O (15 mL), dried over Na_2SO_4, filtered and concentrated under vacuum to yield **9** (537 mg, 2.37 mmol, 100%) as a transparent oil that solidified upon freezing. ^{1}H NMR ($CDCl_3$, 300 MHz): δ 1.44 (s, 9H), 1.65 (m, 1H), 1.92 (m, 2H), 3.16 (q, *J* = 6.6 Hz, 2H) 3.31 (m, 1H), 3.41 (t, *J* = 6.6 Hz, 2H), 4.54 (s, 1H).

***tert*-Butyl (4-(2-amino-6-chloro-9*H*-purin-9-yl)butyl)carbamate (10):** Under an Ar atmosphere, 2-amino-6-chlorpurine (327 mg, 1.93 mmol) was suspended in dry DMF (5 mL) with Cs_2CO_3 (1.43 g, 4.38 mmol) and stirred for 15 minutes. Then, **9** (663 mg, 2.63 mmol) was added to the mixture and stirred for 24 h at room temperature. The reaction was quenched by adding H_2O (5 mL) and the mixture was extracted with AcOEt (4 × 50 mL). The organic layers were pooled, dried over Na_2SO_4, filtrated and concentrated under vacuum. The crude product was purified by flash chromatography (SiO_2, eluent: DCM / EtOH, 98:2, R_f = 0.34) to yield **10** (262 mg, 0.77 mmol, 40%) as a white solid. ^{1}H NMR ($CDCl_3$, 300 MHz): δ 1.45 (s, 9H), 1.52 (m, 2H), 1.77 (m, 2H), 3.21 (q, *J* = 6.4 Hz, 2H), 4.12 (t, *J* = 7.2 Hz, 2H), 4.84 (s, 1H), 5.20 (s, 2H), 7.77 (s, 1H); ^{13}C NMR ($CDCl_3$, 75 MHz): δ 27.1 (CH_2), 28.5 (CH_3 + CH_2), 39.7 (CH_2), 43.3 (CH_2), 77.3 (C_q), 79.6 (C_q), 119.8 (C_q), 125.4 (C_q), 142.4 (CH), 151.5 (C_q), 153.9 (C_q), 156.2 (C_q), 159.2 (C_q); MS (ESI$^+$): *m/z* (%) 341.3 (15) [*M* + H]$^+$, 285.2 (100) [*M* – C_4H_9]$^+$.

6-Chloro-2-methoxy-9-phenoxyacridine (11):[45] PhOH (10.00 g, 106.3 mmol) was mixed with NaOH (400 mg, 10.0 mmol) and 6,9-dichloro-2-methoxyacridine (2.00 g, 7.2 mmol). The mixture was heated up to 120 °C for 2 h and then poured into aq. NaOH (2 M, 50 mL). The aqueous phase was washed with DCM (3 × 40 mL), the organic layers were pooled and dried over Na_2SO_4, filtered and concentrated under vacuum. The crude product was recrystallized from MeOH to yield **11** (960 mg, 2.9 mmol, 40%) as yellow needles. ^{1}H NMR ($CDCl_3$, 300 MHz): δ 3.80 (s, 3H), 6.85 (d, *J* = 7.8, 2H), 7.06 (m, 1H), 7.15 (d, *J* = 2.7 Hz, 1H), 7.28 (m, 2H), 7.36 (dd, *J* = 9.2, 1.9 Hz, 1H), 7.47 (dd, *J* = 9.5, 2.7 Hz, 1H), 7.97 (d, *J* = 9.2, 1H), 8.11 (d, *J* = 9.5, 1H), 8.22 (d, *J* = 1.9 Hz, 1H); ^{13}C NMR ($CDCl_3$, 75 MHz): δ 55.5 (CH_3), 97.7 (CH), 115.6 (CH), 118.8 (C_q), 121.2 (CH), 122.8 (CH), 123.8 (C_q), 126.5 (CH), 127.3 (CH), 128.2

(CH), 130.0 (CH), 131.3 (CH), 135.4 (C_q), 148.5 (C_q), 148.6(C_q), 153.5 (C_q), 157.5 (C_q), 159.0 (C_q); MS (ESI$^+$): *m/z* (%) 336.2 (100) [*M* + H]$^+$.

***N*-(4-(2-amino-6-phenoxy-9*H*-purin-9-yl)butyl)-6-chloro-2-methoxyacridin-9-amine (13):** Compound **10** (171 mg, 0.50 mmol) was dissolved in dry dioxane (4 mL), the reaction was cooled in an ice bath, and HCl (4 M in dioxane, 800 µL, 3.2 mmol) was added and the ice bath immediately removed. Once the reaction reached room temperature, it was gently stirred for 6 h. The solvent was removed under vacuum and the residue was washed with MeOH (10 mL). Then, 6,9-dichloro-2-methoxyacridine (152 mg, 0.45 mmol) and PhOH (800 mg, 10.0 mmol) were added and the mixture was heated for 6 h at 110 °C and then stirred at room temperature for 18 h. The reaction was dissolved in MeOH (1 mL) and Et_2O (10 mL) was added. An orange precipitate was formed. It was collected by filtration and purified by flash chromatography (SiO_2, eluent: DCM / MeOH, 95:5,) to yield compounds **13** (R_f = 0.1, 65 mg, 0.12 mmol, 24%) and **14** (R_f = 0.01 37 mg, 16%) as orange solids. Compound **13**, ^{1}H NMR (DMSO-d_6, 300 MHz): δ 1.79–1.89 (m, 4H), 3.91–4.05 (m, 5H), 4.08 (t, *J* = 5.3 Hz, 2H), 6.35 (s, 2H), 7.21–7.27 (m, 3H), 7.41–7.44 (m, 3H), 7.55 (d, *J* = 7.5 Hz, 1H), 7.75 (s, 1H), 7.73 (d, *J* = 9.3 Hz, 1H), 7.89 (s, 1H), 7.96 (s, 1H), 8.38 (d, *J* = 9.3 Hz, 1H); ^{13}C NMR (APT, DMSO-d_6,75 MHz): δ 26.5 (CH_2), 26.9 (CH_2), 42.4 (CH_2), 48.5 (CH_2), 55.9 (CH_3), 102.3 (CH), 113.4 (C_q), 121.6 (CH), 122.9 (CH), 125.0 (CH),125.6 (CH), 127.6 (CH), 129.5 (CH), 140.8 (CH), 152.3 (C_q), 155.2 (C_q), 155.4 (C_q), 159.6 (C_q); MS (ESI$^+$): *m/z* (%) 540.4 (20) [*M* + H]$^+$, 270.2 (100) [*M* + 2H]$^{2+}$, purity (HPLC): 97%; HRMS (TOF ESI$^+$): calcd for $C_{29}H_{27}ClN_7O_2$ [*M* + H]$^+$: 540.1915, found: 540.1897. The characterization data for compound **14** are given below.

2-Amino-9-(4-((6-chloro-2-methoxyacridin-9-yl)amino)butyl)-1,9-dihydro-6*H*-purin-6-one (14): Compound **15** (159 mg, 0.38 mmol) was dissolved in dry dioxane (5 mL) under an Ar atmosphere and the reaction was cooled on an ice bath. HCl (4 M in dioxane, 500 µL, 2.00 mmol) was added, the ice bath was immediately removed, and the reaction was stirred for 2.5 h until the disappearance of the starting material (TLC). The solvent was removed under vacuum and PhOH (700 mg, 9.09 mmol) and 6,9-dichloro-2-methoxyacridine (118 mg, 0.31 mmol) were added. The reaction was heated for 4 h at 110 °C and then stirred at room temperature for 24 h. After cooling, Et_2O (50 mL) was added, the orange precipitate was collected and purified by flash chromatography (SiO_2, eluent: DCM / MeOH / TEA, 95:5:1, R_f = 0.1). Compound **14** (90 mg, 0.19 mmol, 50%) was obtained as an orange solid; ^{1}H NMR (300 MHz, DMSO-d_6): δ 1.69–1.80 (m, 4H), 3.79 (t, *J* = 6.9 Hz, 2H), 3.75–3.96 (m, 5H), 6.40 (s, 2H), 7.06 (br s, 1H), 7.33 (dd, *J* = 9.3, 1.5 Hz, 1H), 7.43 (dd, *J* = 9.3, 2.0 Hz), 7.60 (d, *J* = 2.3 Hz, 1H), 7.65 (s, 1H), 7.81–7.87 (m, 3H), 8.30 (d, *J* = 9.3 Hz, 1H), 10.53 (s, 1H); ^{13}C NMR (DMSO-d_6, 75 MHz): δ 26.5 (CH_2), 28.0 (CH_2), 42.3 (CH_2), 49.0 (CH_2), 55.6 (CH_3), 116.6 (CH), 117.0 (C_q), 119.2 (CH); 122.7 (CH), 126.6 (CH), 133.8 (CH), 137.4 (C_q), 150.7 (C_q), 151.1 (C_q),

153.4 (C_q), 155.1 (C_q), 156.8 (C_q); MS (ESI$^+$): *m/z* (%) 232.7 (100) [*M* + 2H]$^{2+}$, 464.4 (15) [*M* + H]$^+$, purity (HPLC): 98%; HRMS (ESI$^+$ TOF) calcd for $C_{23}H_{23}ClN_7O_2$ [*M* + H]$^+$: 464.1602, found: 464.1577.

***tert*-Butyl (4-(2-amino-6-(benzyloxy)-9*H*-purin-9-yl)butyl)carbamate (15):** BG (315 mg, 1.31 mmol) was suspended with Cs_2CO_3 (851 mg, 2.61 mmol) in dry DMF (10 mL) and stirred under an Ar atmosphere for 10 minutes. Then, compound **9** (395 mg, 1.56 mmol) was added and the mixture was stirred for 24 h at room temperature. To quench the reaction, H_2O (15 mL) was added and the mixture was extracted with AcOEt (4 × 25 mL). The organic layers were pooled, dried over Na_2SO_4, filtrated and concentrated under vacuum. The residue was purified by flash chromatography (SiO_2, eluent: DCM / MeOH gradient, 100:0 to 98:2, R_f = 0.3) to yield **15** (247 mg, 0.60 mmol, 46%) as a transparent oil that solidified in the fridge. ^{1}H NMR ($CDCl_3$, 300 MHz): δ 1.45 (s, 9H), 1.50 (m, 2H), 1.89 (m, 2H), 3.20 (dd, *J* = 8.5, 6.7 Hz, 2H), 4.07 (t, *J* = 6.8 Hz, 2H), 4.90 (s, 2H), 5.06 (s, 1H), 5.57 (s, 2H), 7.26–7.52 (m, 5H), 7.59 (s, 1H); ^{13}C NMR ($CDCl_3$, 75 MHz): δ 26.7 (CH_2), 27.3 (CH_2), 28.4 (CH_3), 39.7 (CH_2), 42.8 (CH_2), 68.0 (CH_2), 79.0 (CH_q), 115.6 (C_q), 127.9 (CH), 128.2 (CH), 128.4 (CH), 136.5 (C_q), 139.2 (CH), 154.1 (C_q), 156.1 (C_q), 159.2 (C_q), 161.0 (C_q); HRMS (TOF ESI$^+$): calcd for $C_{21}H_{30}N_6O_3$ [*M* + H]$^+$: 413.2296, found: 413.2277.

***N*-(2-(2-(2-Iodoethoxy)ethoxy)ethyl)phthalimide (16c):** Potassium phthalimide (1.00 g, 5.40 mmol) was suspended in 1,2-bis(2-chloroethoxy)ethane (8.5 mL, 10.1 g, 54.0 mmol) under an Ar atmosphere and the mixture was heated at 130 °C for 48 h. The reaction mixture was cooled and directly purified by flash chromatography (SiO_2, eluent: cyclohexane / AcOEt, 8:2 to 6:4, R_f = 0.2 in 7:3) to yield ***N*-(2-(2-(2-chloroethoxy)ethoxy)ethyl)phthalimide** [48] (**16d**, 957 mg, 3.3 mmol, 61%) as a transparent oil; ^{1}H NMR ($CDCl_3$, 300 MHz): δ 3.54 (t, *J* = 5.4 Hz, 2H), 3.56–3.70 (m, 6H), 3.75 (t, *J* = 5.6 Hz, 2H), 3.91 (t, *J* = 5.6 Hz, 2H), 7.73–7.75 (m, 2H), 7.84–7.86 (m, 2H); ^{13}C NMR (APT, $CDCl_3$, 75 MHz): δ 37.3 (CH_2), 42.7 (CH_2), 68.0 (CH_2), 70.1 (CH_2), 70.6 (CH_2), 71.4 (CH_2), 123.3 (CH), 132.1 (CH), 133.9 (C_q), 168.3 (C_q). MS (ESI$^+$): *m/z* (%) 298.3 (10) [*M* + H]$^+$, 174.2 (100) [*M* – $C_4H_8ClO_2$]$^+$. Intermediate **16d** (200 mg, 0.67 mmol) and NaI (252 mg, 2.67 mmol) were dissolved in dry MeCN (4 mL) under an Ar atmosphere and refluxed for 24 h. The reaction was quenched by addition of H_2O (10 mL) and the mixture was extracted with AcOEt (4 × 10 mL). The organic layers were pooled, dried over Na_2SO_4, filtered and concentrated in vacuum to yield compound **16c** (251 mg, 0.64 mmol, 96%) as a yellow oil which was used without further purification; ^{1}H NMR ($CDCl_3$, 300 MHz): δ 3.17 (t, *J* = 6.9 Hz, 2H), 3.60–3.68 (m, 6H), 3.76 (t, *J* = 5.7 Hz, 2H), 3.91 (t, *J* = 5.7 Hz, 2H), 7.71–7.73 (m, 2H), 7.83–7.87 (m, 2H); ^{13}C NMR (APT, $CDCl_3$, 75 MHz): δ 3.00 (CH_2), 37.4 (CH_2), 68.1 (CH_2), 70.2 (CH_2), 70.3 (CH_2), 72.1 (CH_2), 123.4 (CH), 132.3 (CH), 134.1 (C_q),

168.4 (C_q); MS (ESI$^+$): *m/z* (%) 412.2 (5) [*M* + Na]$^+$, 390.2 (30) [*M* + H]$^+$, 362.1 (40) [*M* – I]$^+$, 174.2 (100) [*M* – $C_4H_8IO_2$]$^+$.

***N*-(4-(2-Amino-6-(benzyloxy)-9*H*-purin-9-yl)butyl)phthalimide (17a)** [89]**:** BG (1.50 g, 6.24 mmol) and Cs_2CO_3 (3.00 g, 9.30 mmol) were suspended in dry DMF (20 mL) under an Ar atmosphere and the mixture was stirred for 10 minutes. *N*-(4-bromobutyl)phthalimide (**16a**, 1.90 g, 6.81 mmol) was added and the reaction was stirred at room temperature for 24 h. The reaction was quenched by addition of H_2O (10 mL), extracted with AcOEt (3 × 100 mL), the organic layers were pooled, dried over Na_2SO_4, filtered and concentrated in vacuum. The residue was purified by flash chromatography (SiO_2, eluent: DCM / MeOH, 98:2, R_f = 0.14) to give **17a** (1.90 g, 4.22 mmol, 68%) as a white solid. ^{1}H NMR ($CDCl_3$, 300 MHz): δ 1.72 (m, 2H), 1.90 (m, 2H), 3.75 (t, *J* = 7.3 Hz, 2H), 4.11 (t, *J* = 7.0 Hz, 2H), 4.84 (s, 2H), 5.56 (s, 2H), 7.29–7.35 (m, 3H), 7.50 (m, 2H), 7.60 (s, 1H), 7.72 (dd, *J* = 5.4, 3.0 Hz, 2H), 7.83 (dd, *J* = 5.4, 3.0 Hz, 2H); ^{13}C NMR ($CDCl_3$, 75 MHz): δ 25.6 (CH_2), 27.2 (CH_2), 37.0 (CH_2), 42.8 (CH_2), 67.9 (CH_2), 115.7 (C_q), 123.3 (CH), 127.9 (CH), 128.2 (CH), 128.4 (CH), 132.0 (CH), 134.0 (CH), 136.5 (C_q), 139.4 (CH), 154.2 (C_q), 159.2 (C_q), 161.0 (C_q), 168.4 (C_q); MS (ESI$^+$): *m/z* (%) 443.3 (100) [*M* + H]$^+$, purity (HPLC): 96%; HRMS (ESI$^+$ TOF) calcd for $C_{24}H_{23}N_6O_3$ [*M* + H]$^+$: 443.1832, found: 443.1819.

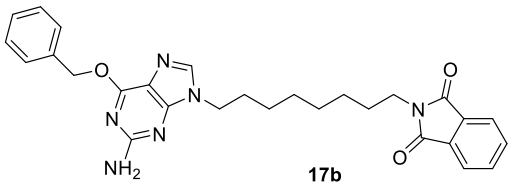

17b

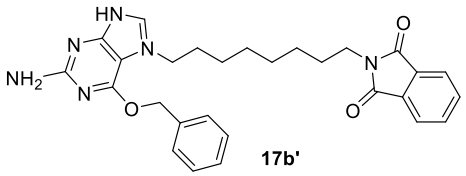

17b'

***N*-(8-(2-Amino-6-(benzyloxy)-9*H*-purin-9-yl)octyl)phthalimide (17b):** BG (1.00 g, 4.14 mmol) was dissolved in dry DMF (20 mL) under an Ar atmosphere and the solution was cooled to 0 °C. Cs_2CO_3 (2.00 g, 6.14 mmol) and *N*-(8-bromooctyl)phthalimide (**16b**, 1.70 g, 4.91 mmol) was added in portions. The reaction was kept on an ice bath for 8 h and then stirred at room temperature for a total of 24 h. The reaction was quenched by the addition of H_2O (40 mL), extracted with AcOEt (6 x 40 mL), the organic layers were pooled, dried over Na_2SO_4, filtered and concentrated in vacuum. The residue was purified by flash chromatography (SiO_2, eluent: DCM / EtOH, 99:1 to 97:3, R_f = 0.36 and 0.28 in 95:5 for N^9 and N^7 isomers respectively). The N^9 and N7 isomers were assigned according to the correlations observed in HMBC spectra. The N^9 isomer (**17b**, 998 mg, 2.01 mmol, 48%) was obtained as a white solid; ^{1}H NMR ($CDCl_3$,

300 MHz): δ 1.32 (m, 8H), 1.66 (m, 2H), 1.82 (m, 2H), 3.67 (t, *J* = 7.2 H, 2H), 4.03 (t, *J* = 7.2 Hz, 2H), 4.86 (s, 2H), 5.56 (s, 2H), 7.32–7.37 (m, 3H), 7.50–7.52 (m, 2H), 7.59 (s, 1H), 7.69–7.72 (2H), 7.81–7.85 (m, 2H); ^{13}C NMR (APT, $CDCl_3$, 75 MHz): δ 26.6 (CH_2), 26.8 (CH_2), 28.6 (CH_2), 28.9 (CH_2), 29.0 (CH_2), 29.9 (CH_2), 38.1 (CH_2), 43.6 (CH_2), 68.1 (CH_2), 115.8 (CH), 123.3 (CH), 128.0 (CH), 128.4 (CH), 128.5 (CH), 132.2 (C_q), 134.0 (CH), 136.7 (C_q), 139.6 (CH), 154.3 (C_q), 159.2 (C_q), 161.1 (C_q), 168.6 (C_q); MS (ESI$^+$): *m/z* (%) 499.4 (100) [*M* + H]$^+$ (100). The *N*^{7} isomer (**17b′**, 608 mg, 1.21 mmol, 24%) was obtained as a white solid; ^{1}H NMR ($CDCl_3$, 300 MHz): δ 1.18–1.22 (m, 4H), 1.23–1.25 (m, 4H), 1.64 (dd, *J* = 7.3, 6.7 Hz, 2H), 1.75 (dd, *J* = 7.3, 7.1 Hz, 2H), 3.66 (t, *J* = 7.3 Hz, 2H), 4.12 (t, *J* = 7.3 Hz, 2H), 4.98 (s, 2H), 5.5 (s, 2H), 7.35–7.45 (m, 5H), 7.39–7.71 (dd, *J* = 5.4, 3.1 Hz, 2H), 7.74 (s, 1H), 7.82 (dd, *J* = 5.4, 3.1 Hz, 2H); ^{13}C NMR (APT, $CDCl_3$, 75 MHz): δ 26.3 (CH_2), 26.7 (CH_2), 28.5 (CH_2), 28.8 (CH_2), 28.9 (CH_2), 31.3 (CH_2), 38.0 (CH_2), 47.6 (CH_2), 68.2 (CH_2), 107.2 (C_q), 123.2 (CH), 128.2 (CH), 128.4 (CH), 128.7 (CH), 132.2 (C_q), 134.0 (CH), 136.2 (C_q), 144.7 (CH), 157.2 (C_q), 159.3 (C_q), 164.1 (C_q), 164.4 (C_q); MS (ESI$^+$): *m/z* (%) 499.4 (100) [*M* + H]$^+$ (100).

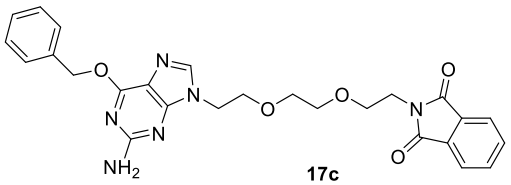

17c

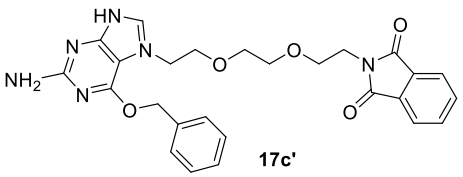

17c'

***N*-(2-(2-(2-(2-Amino-6-(benzyloxy)-9*H*-purin-9-yl)ethoxy)ethoxy)ethyl)phthalimide (17c):** BG (366 mg, 1.52 mmol) was dissolved in dry DMF (14 mL) under an Ar atmosphere. The solution was cooled to 0 °C in an ice bath, and Cs_2CO_3 (731 mg, 1.52 mmol) and compound **16c** (708 mg, 1.82 mmol) in dry DMF (6 mL) was added in portions. The reaction mixture was stirred at 0 °C for 8 h and then at room temperature for 24 h. The reaction was quenched by adding H_2O (40 mL) and the mixture was extracted with AcOEt (6 × 40 mL). The organic layers were pooled, dried over Na_2SO_4, filtered and concentrated in vacuum. The residue was purified by flash chromatography (SiO_2, eluent: DCM / EtOH, 99:1 to 96:4, R_f = 0.4 and 0.17 for 98:2 for *N*^{9} and *N*^{7} isomers respectively). The *N*^{9} and N7 isomers were assigned according to the correlations observed in HMBC spectra. The *N*^{9} isomer (**17c**, 277 mg, 0.55 mmol, 36%) was obtained as a sticky oil; ^{1}H NMR ($CDCl_3$, 300 MHz): δ 3.53 (m, 2H), 3.58 (m, 2H), 3.70 (m, 4H), 3.88 (t, *J* = 5.6 Hz, 2H), 4.16 (t, *J* = 4.9 Hz, 2H), 4.85 (s, 2H), 5.56 (s, 2H), 7.26–7.29 (m, 3H), 7.49–7.52 (m, 2H), 7.69–7.72 (m, 3H), 7.82–7.85 (m, 2H); ^{13}C NMR (APT, $CDCl_3$, 75

MHz): δ 37.2 (CH_2), 43.3 (CH_2), 68.0 (CH_2), 68.1 (CH_2), 69.3 (CH_2), 70.0 (CH_2), 70.6 (CH_2), 115.4 (C_q) 123.3 (CH), 127.9 (CH), 128.3 (CH), 128.4 (CH), 132.1 (C_q), 133.9 (CH), 136.6 (C_q), 140.6 (CH), 154.1 (C_q), 159.1 (C_q), 161.0 (C_q), 168.3 (C_q); MS (ESI^+): *m/z* (%): 503.4 (100) $[M + H]^+$. Isomer N^7 (**17c′**, 280 mg, 0.56 mmol, 37%) was obtained as a sticky oil; ^1H NMR ($CDCl_3$, 300 MHz): δ 3.41 (dd, *J* = 5.6, 3.0 Hz, 2H), 3.5 (dd, *J* =5.6, 3.0 Hz, 2H), 3.68 (m, 4H), 3.84 (t, *J* = 5.4 Hz, 2H), 4.29 (t, *J* = 5.7 Hz, 2H), 4.90 (s, 2H), 5.05 (s, 2H), 7.35–7.44 (m, 5H), 7.67–7.69 (m, 2H), 7.79–7.83 (m, 2H), 7.85 (s, 1H); ^{13}C NMR (APT, $CDCl_3$, 75 MHz): δ 37.2 (CH_2), 47.2 (CH_2), 68.0 (CH_2), 69.8 (CH_2), 69.9 (CH_2), 70.6 (CH_2), 106.8 (C_q), 123.2 (CH), 128.1 (CH), 128.3 (C_q), 128.6 (CH), 132.1 (CH), 133.9 (CH), 136.2 (C_q), 145.9 (CH), 157.1 (C_q), 159.1 (C_q), 164.1 (C_q), 166.8 (C_q); MS (ESI^+): *m/z* (%) 503.4 (100) $[M + H]^+$.

9-(4-Aminobutyl)-6-(benzyloxy)-9*H*-purin-2-amine (18a) [89]**:** Compound **17a** (1.42 g, 3.19 mmol) was dissolved in EtOH (80 mL) together with hydrazine hydrate (1.55 mL, 1.59 g, 31.9 mmol). The mixture was heated at 65 °C for 2.5 h. The reaction mixture was cooled and filtrated. The filtrate was concentrated under vacuum and the residue was suspended in DCM (20 mL), re-filtered, and the filtrate was concentrated in vacuum. The crude residue was purified by flash chromatography (SiO_2, eluent: DCM / MeOH / TEA, 85:15:1, R_f = 0.11) to yield compound **18a** (815 mg, 2.61 mmol, 82%) as a white solid which was stored under Ar at –20 °C. ^1H NMR ($CDCl_3$, 300 MHz): δ 1.42–1.52 (m, 2H), 1.84–1.95 (m, 4H), 2.73 (t, *J* = 6.9 Hz, 2H), 4.07 (t, *J* = 7.2 Hz, 2H), 4.90 (s, 2H), 5.56 (s, 2H), 7.30–7.52 (m, 5H), 7.59 (s, 1H); ^{13}C NMR (APT, $CDCl_3$, 75 MHz): δ 27.4 (CH_2), 30.6 (CH_2), 41.6 (CH_2), 43.4 (CH_2), 68.1 (CH_2), 115.6 (C_q), 128.1 (CH), 128.4 (CH), 128.5 (CH), 136.6 (C_q), 139.5 (CH), 154.3 (C_q), 159.3 (C_q), 161.1 (C_q); MS (ESI^+): *m/z* (%) 313.2 (60) $[M + H]^+$, 242.1 (80) $[M – C_4H_{10}N]^+$, 152.2 $[M – C_4H_{10}N – Bn]^+$; purity (HPLC): 100%; HRMS (ESI^+ TOF) calcd for $C_{16}H_{21}N_6O$ $[M + H]^+$: 313.1777, found: 317.1786.

9-(8-Aminooctyl)-6-(benzyloxy)-9*H*-purin-2-amine (18b): Compound **17b** (400 mg, 0.80 mmol) was dissolved in EtOH (10 mL) together with hydrazine hydrate (382 µL, 400 mg, 0.80 mmol). The reaction was heated for 1 h at 65 °C and cooled to room temperature. The reaction mixture was filtered, and the white solid was washed with DCM (2 × 10 mL). The filtrate was concentrated under vacuum, resuspended in DCM (20 mL), then filtered again and the filter cake was washed with DCM (2 × 10 mL). The filtrate was concentrated in vacuum to yield compound **18b** (278 mg, 0.75 mmol, 94%) as a sticky yellow oil which was used without further purification. ^1H NMR ($CDCl_3$, 300 MHz): δ 1.26 (m, 8H), 1.38–1.40 (m, 2H), 1.78–1.83 (m, 2H), 2.09 (br s, 2H), 2.63 (t, *J* = 7.0 Hz, 2H), 4.01 (t, *J* = 7.2 Hz, 2H), 5.14 (s, 2H), 5.55 (s, 2H), 7.23–7.31 (m, 3H), 7.48–7.50 (m, 2H), 7.58 (s, 1H); ^{13}C NMR (APT, $CDCl_3$, 75 MHz): δ 26.4 (CH_2), 26.6 (CH_2), 28.9 (CH_2), 29.1 (CH_2), 29.7 (CH_2), 33.4 (CH_2), 41.9 (CH_2), 43.5 (CH_2), 67.9

(CH_2), 115.5 (C_q), 127.9 (CH), 128.1 (CH), 128.3 (CH), 136.5 (C_q), 139.4 (CH), 154.1 (C_q), 159.2 (C_q), 160.9 (C_q); MS (ESI^+): *m/z* (%) 369.2 (100) $[M + H]^+$.

9-(2-(2-(2-aminoethoxy)ethoxy)ethyl)-6-(benzyloxy)-9*H*-purin-2-amine (18c): Compound **17c** (277 mg, 0.55 mmol) was dissolved in EtOH (8 mL) together with hydrazine hydrate (300 µL, 315 mg, 6.1 mmol). The reaction was heated for 1 h at 65 °C and cooled to room temperature. The reaction mixture was filtered, and the white solid was washed with DCM (2 × 10 mL). The filtrate was concentrated under vacuum, suspended in DCM (20 mL), filtered again, and the filter cake was washed with DCM (2 × 10 mL). The filtrate was concentrated in vacuum to yield compound **18c** (195 mg, 0.52 mmol, 95%) as a sticky oil which was used without further purification. ^{1}H NMR ($CDCl_3$, 300 MHz): δ 2.11 (br s, 2H), 2.84 (t, *J* = 5.2 Hz, 2H), 3.38 (t, *J* = 5.2 Hz, 2H), 3.5 (m, 4H), 3.79 (t, *J* = 5.1 Hz, 2H), 4.24 (t, *J* = 5.1 Hz, 2H), 4.94 (s, 2H), 5.56 (s, 2H), 7.30–7.33 (m, 3H), 7.49–7.52 (m, 2H), 7.76 (s, 1H); ^{13}C NMR (APT, $CDCl_3$, 75 MHz): δ 41.7 (CH_2), 43.4 (CH_2), 68.1 (CH_2), 69.4 (CH_2), 70.3 (CH_2), 70.7 (CH_2), 73.4 (CH_2), 115.4 (C_q), 128.0 (CH), 128.4 (CH), 128.5 (CH), 136.6 (C_q), 140.6 (CH), 154.2 (C_q), 159.3 (C_q), 161.1 (C_q); MS (ESI^+): *m/z* (%) 373.3 (100) $[M + H]^+$.

***N*-(4-(2-amino-6-(benzyloxy)-9*H*-purin-9-yl)butyl)-6-chloro-2-methoxyacridin-9-amine (19a):** Compounds **18a** (200 mg, 0.64 mmol) and **11** (195 mg, 0.58 mmol) were dissolved in dry pyridine (5 mL) under an Ar atmosphere and the mixture was refluxed for 24 h. The solvent was removed in vacuum and the residue was purified by flash chromatography (SiO_2, eluent: DCM / MeOH, 99:1 to 93:7; R_f = 0.12 at a 93:7 ratio) to yield compound **19a** (200 mg, 0.36 mmol, 56%) as an orange solid. ^{1}H NMR ($CDCl_3$, 300 MHz): δ 1.26 (s, 1H), 1.82 (m, 2H), 1.98 (m, 2H), 3.79 (m, 2H), 3.88 (s, 3H), 4.12 (t, *J* = 6.7 Hz, 1H), 4.87 (s, 2H), 5.56 (s, 2H), 7.23–7.35 (m, 6H), 7.51 (m, 2H), 7.5 (s, 1H), 7.97 (m, 2H), 8.0 (d, *J* = 1.3 Hz, 1H); ^{13}C NMR (APT, $CDCl_3$, 75 MHz): δ 27.6 (CH_2), 28.7 (CH_2), 43.1 (CH_2), 50.0 (CH_2), 55.7 (CH_3), 68.2 (CH_2), 68.1 (CH_2), 99.2 (CH), 115.8 (C_q), 116.2 (C_q), 118.4 (C_q), 124.1 (CH), 124.7 (CH), 124.9 (CH), 128.2 (CH), 128.4 (CH), 128.5 (CH), 131.2 (CH), 135.1 (C_q), 136.5 (C_q), 139.3 (CH), 143.6 (C_q), 149.7 (C_q), 154.2 (C_q), 156.3 (C_q), 159.3 (C_q), 161.2 (C_q); MS (ESI^+): *m/z* (%) 554.3 (60) $[M + H]^+$, 464.2 (100) $[M – Bn]^+$, purity (HPLC): 95%; HRMS (ESI^+ TOF) calcd for $C_{30}H_{29}ClN_7O_2$ $[M + H]^+$: 554.2071, found: 554.2060.

***N*-(8-(2-amino-6-(benzyloxy)-9*H*-purin-9-yl)octyl)-6-chloro-2-methoxyacridin-9-amine (19b):** Compounds **18b** (278 mg, 0.75 mmol) and **11** (295 mg, 0.89 mmol) were dissolved in dry pyridine (10 mL) under an Ar atmosphere and the mixture was refluxed for 24 h. The solvent was removed in vacuum and the residue was purified by flash chromatography (SiO_2, eluent: DCM / MeOH, 98:2 to 95:5, R_f = 0.16 at a 95:5 ratio) to yield compound **19b** (123 mg, 0.20 mmol, 25%) as an orange solid; ^{1}H NMR ($MeOD_4$, 300 MHz): δ 1.15–1.30 (m, 10H),

1.72–7.76 (m, 4H), 3.79 (t, *J* = 7.1 Hz, 2H), 3.93 (s, 3H), 4.02 (t, *J* = 7.1 Hz, 2H), 5.50 (s, 2H), 7.25–7.35 (m, 4H), 7.40 (dd, *J* = 2.6, 9.2 Hz, 1H), 7.46–7.48 (m, 2H), 7.50 (d, *J* = 2.6 Hz, 1H), 7.76–7.81 (m, 3H), 8.23 (d, *J* = 9.2 Hz, 1H); ^{13}C NMR (APT, $MeOD_4$, 75 MHz): δ 27.4 (CH_2), 27.7 (CH_2), 29.9 (CH_2), 30.0 (CH_2), 30.6 (CH_2), 31.8 (CH_2), 44.5 (CH_2), 56.2 (CH_3), 68.9 (CH_2), 101.6 (CH), 115.2 (C_q), 118.0 (C_q), 124.3 (CH), 125.8 (CH), 126.4 (CH), 127.4 (CH), 129.1 (CH), 129.3 (CH), 129.4 (CH), 137.2 (C_q), 137.9 (C_q), 141.2 (CH), 145.4 (C_q), 148.2 (C_q), 153.7 (C_q), 155.1 (C_q), 157.3 (C_q), 161.6 (C_q), 162.0 (C_q). MS (ESI$^+$): *m/z* (%) 610.4 (40) [*M* + H]$^+$, 520.4 (100) [*M* – Bn]$^+$, purity (HPLC): 98%; HRMS (ESI$^+$ TOF) calcd for $C_{34}H_{37}ClN_7O_2$ [*M* + H]$^+$: 610.2697, found: 610.2725.

***N*-(2-(2-(2-(2-amino-6-(benzyloxy)-9*H*-purin-9-yl)ethoxy)ethoxy)ethyl)-6-chloro-2-methoxyacridin-9-amine (19c):** Compounds **18c** (195 mg, 0.52 mmol) and **11** (180 mg, 0.54 mmol) were dissolved in dry pyridine (8 mL) under an Ar atmosphere and the mixture was refluxed for 24 h. The solvent was removed in vacuum and the residue was purified by flash chromatography (SiO_2, eluent: DCM / MeOH, 98:2 to 95:5, R_f = 0.19 at a 90:10 ratio) to yield compound **19c** (91 mg, 0.15 mmol, 27%) as an orange solid; ^{1}H NMR ($MeOD_4$, 300 MHz): δ 3.55 (s, 4H), 3.63 (t, *J* = 5.1 Hz, 2H), 3.74 (t, *J* = 4.9 Hz, 2H), 3.85–7.87 (m, 5H), 4.43 (t, *J* = 4.9 Hz, 2H), 5.28 (s, 2H), 7.19–7.33 (m, 6H), 7.37–7.40 (m, 2H), 7.71–7.76 (m, 3H), 8.14 (d, *J* = 8.1 Hz, 1H); ^{13}C NMR (APT, $MeOD_4$, 75 MHz): δ 42.7 (CH_2), 49.1 (CH_2), 54.9 (CH_3), 67.5 (CH_2), 68.4 (CH_2), 69.8 (CH_2), 69.9 (2 × CH_2), 100.4 (CH), 113.4 (C_q), 114.4 (C_q), 117.1 (C_q), 123.4 (CH), 124.0 (CH), 125.3 (CH), 125.8 (CH), 127.2 (CH), 127.6 (CH), 127.8 (CH), 127.9 (CH), 136.1 (C_q), 136.3 (C_q), 140.4 (CH), 143.4 (C_q), 145.9 (C_q), 152.6 (C_q), 153.6 (C_q), 156.0 (C_q), 160.2 (C_q), 160.4 (C_q); MS (ESI$^+$): *m/z* (%) 614.3 (50) [*M* + H]$^+$, 524.3 (100) [*M* – Bn]$^+$ (100), purity (HPLC): 96%; HRMS (ESI$^+$ TOF) calcd for $C_{34}H_{37}ClN_7O_2$ [*M* + H]$^+$: 614.2283, found: 614.2341.

5.2. Absorption and fluorescence spectroscopy

UV spectra were recorded either on a Hitachi U2900 or (in the case of varied-temperature experiments) on a Cary 300 Bio double-beam spectrophotometers, in quartz cuvettes (1 cm path length). Ligand concentration was 10 μM, with a maximum of 0.2% (v/v) DMSO. Hypochromism (*H*) values were determined using Equation (1):

$$H\,(\%) = 100 \times \left(1 - \frac{f(\text{hybrid})}{f(\text{BG}) + f(\mathbf{8})}\right), \qquad (1)$$

where *f* is the oscillator strength, obtained by integration of the corresponding absorption spectrum in the 260–315 nm region [49]. Fluorescence spectra were recorded on a HORIBA

JobinYvon Fluoromax-3 spectrofluorimeter in quartz cuvettes (10 × 10 mm path) at a 1 μM ligand concentration with a maximum of 0.2% (v/v) DMSO, using the following parameters: λ_{exc} = 424 nm, integration time: 0.5 s, excitation / emission slits: 5 nm. Fluorescence quantum yields were calculated using a solution of Coumarin 153 in EtOH as a standard (Φ = 0.38) [51].

5.3. DNA-binding studies

Spectrophotometric titrations: Calf thymus DNA (CT DNA, Invitrogen, 10 mg mL^{-1}) was diluted ≈ 5-fold with 10 mM $LiAsO_2Me_2$, 100 mM KCl buffer, pH 7.2 and the precise concentration (3 mM base pairs, bp) was determined through $A_{260\ nm}$ measurement using the extinction coefficient value of 12,824 cm^{-1} M^{-1}. UV/Vis titrations were performed by titrating ligand solutions (c = 20 μM in 10 mM $LiAsO_2Me_2$, 100 mM KCl buffer, pH 7.2) with solutions of CT DNA (3 mM) supplemented with 20 μM of the respective ligand to avoid the dilution effects). After 5 min equilibration at room temperature, spectra were recorded in the 350–500 nm range and binding isotherms were plotted as A / A_0 at 410 nm *vs.* c(CT DNA) and fitted to a One Site Binding model (Equation 2) in GraphPad Prism:

$$Y=B_{max} \times X / (K_d + X), \quad (2)$$

where X = c(CT DNA) and K_d is the equilibrium dissociation constant. The results represent the K_d values ± s.d. from three to five replicates.

Thermal denaturation experiments: Samples containing CT DNA (12.5 μM bp) and compounds (6.25 μM) or DMSO control (0.6% v/v) in 10 mM $KAsO_2Me_2$, pH 7.2 buffer (total volume: 1000 μL) were degassed, placed into self-masked quartz cuvettes (path length: 1 cm), sealed and heated from 20 to 95 °C at a rate of 0.2 °C min^{-1}, while the absorption was measured at 260 nm, with a Cary 300 Bio spectrophotometer. Melting temperatures (T_m) were determined as maxima of first-order derivatives of melting curves using Cary WinUV software. The experiments were performed in triplicate.

Ethidium bromide (EB) displacement assay: Experiments were performed based on the already described protocols [90]. Briefly, EB solution in 10 mM $LiAsO_2Me_2$, 100 mM KCl buffer, pH 7.2 (1.13 μM, 44 μL), CT DNA solution in the same buffer (20 μM bp, 5 μL) and compound solution in DMSO (0–1 mM, 1 μL) were mixed in a 96-well half-area black, flat-bottom NBS microplate (Corning 3993) and incubated for 30 min at room temperature in the dark. Fluorescence was measured on a microplate reader (CLARIOstar^{Plus}, BMG Labtech) using excitation at 545 nm (bandwidth: 15 nm) and emission at 595 nm (bandwidth: 20 nm). Fluorescence intensity, corrected for the background fluorescence of EB in the absence of

DNA, was plotted as a function of compound concentration. Results are the means from 3–5 independent titrations with their corresponding standard deviations.

Circular dichroism spectroscopy: CD spectra were recorded on a JASCO J-1500 spectropolarimeter. A 3 mL solution containing the compounds **8** or **19c** (50 µM) and CT DNA (500 µM bp) in 10 mM $LiAsO_2Me_2$, 100 mM KCl buffer, pH 7.2, was prepared and spectra were recorded in quartz cuvettes (1 cm path length) in a 300–500 nm range (bandwidth: 2 nm, scanning speed: 100 nm min^{-1}, 8 scans per sample) at room temperature. Spectra were corrected by blank subtraction.

5.4. *In vitro* MGMT inhibition assays

Oligonucleotides and protein solutions: RP-HPLC purified and lyophilized DNA oligonucleotides (Table 5) were purchased from Eurogentec (Seraign, Belgium), reconstituted in sterile water to a concentration of 100 µM according to the manufacturer's indications, and stored at –20 °C when not in use.

Table 5. Oligonucleotides used in this work.

Acronym	Sequence (5′ → 3′)
S1	Cy3-TAAAAGACTTC(O^6MeG)AAAAATTTTTAAAA
S2	TTTTAAAAATTTTTCGAAGTCTTTTA
S1′	Cy3-TAAAAGACTTCGAAAAATTTTTAAAA
Q1	GGGTTACT(O^6MeG)CGAACTGG
Q2	CCAGTTCGCAGTAACCC

For preparation of the O^6MeG-bearing substrate (S) or the non-methylated control (S′) duplexes, the Cy3-labelled 26-mers S1 or S1′ respectively (final concentration: 6.4 µM) were mixed with a slight excess of the unlabeled complementary strand S2 (final concentration: 7.0 µM) in a 10 mM Tris-HCl, 100 mM NaCl buffer (pH 8.5). For preparation of the unlabeled quencher (Q), the complementary 17-mers Q1 and Q2 were mixed in the same buffer to give the final concentration of each strand of 15 µM. The duplexes were annealed by heating for 5 min at 90 °C and then left to reach room temperature within ~ 3 h. CT DNA (10 mg mL^{-1}) was diluted 20-fold with the same buffer and the precise concentration (700 µM) was determined through $A_{260\ nm}$ measurement. Except from single stranded DNA, all solution were stored at + 4 °C covered from light.

MGMT protein: Recombinant human MGMT was produced and purified following a modification of the published protocol [91]. Human MGMT cDNA was digested with restriction endonucleases BamHI and XhoI and ligated into pET24 vector. *E. coli* STAR BL 21 pRare cells were transformed and grown at 37 °C in 1 L of Terrific Broth. Overexpression was induced with 0.25% arabinose and 0.5 mM IPTG at 20 °C overnight. The cells were harvested by centrifugation at 4000 × *g*, 4 °C for 15 min. The pellets were suspended in lysis buffer (glycerophosphate pH 7.6 50 mM, NaCl 80 mM, β-mercaptoethanol 8 mM, $MgCl_2$ 1 mM, *S. marcescens* nuclease (benzonase) 170 U μl^{-1}, 1X complete EDTA-free protease inhibitor cocktail). Cells were disrupted by passage through a T75 cell disruptor (Constant Systems, CellD). The resulting cell lysate was centrifuged at 43,000 × *g*, 4 °C for 1 h. Solid ammonium sulfate was added to the supernatant fraction to a final concentration of 25%. The mixture was stirred on ice for 15 min and left to stand on ice for 30 min. The precipitate was removed by centrifugation at 20,000 × *g*, 4 °C for 20 min. Additional ammonium sulfate was added to the supernatant to a final concentration of 55%. After a second centrifugation, the precipitate was redissolved in Buffer A (Tris-HCl pH 8.4 50 mM, EDTA 1 mM, β-mercaptoethanol 2 mM) and subjected to affinity chromatography on Toyopearl AF-Red (Tosoh Bioscience). The proteins were eluted in a buffer composed in Buffer A and NaCl (2 M). After an overnight dialysis (Spectra/Por 3, MWCO 3.5 kDa) against Buffer C (Tris-HCl 50 mM pH 8, EDTA 1 mM, glycerol 10%, DTT 1 mM, NaCl 20 mM), the eluate was loaded onto a Capto SP ImpRes ion exchange column (Cytiva) and eluted with a continuous gradient of NaCl (0.02 to 1 M) in the same buffer. The fractions containing MGMT were pooled, dialyzed and concentrated (Macrosep Pall, MWCO 3 kDa) with a buffer C (Tris-HCl 50 mM pH 8, EDTA 1 mM, glycerol 10%, DTT 1 mM, NaCl 500 mM) to a volume of about 3 mL, loaded onto a size exclusion chromatography column (HiLoad Superdex 75 pg, 26 × 600, Cytiva) and eluted with buffer C. The fractions containing the protein were collected. The purity of the protein was visualized on a 4–20% SDS-PAGE. The protein concentration (8 µM) was determined by $OD_{280\ nm}$ measurement. The enzyme was stored at –80 °C.

Coupled enzymatic assay: Stock solutions of compounds were prepared in DMSO at a 10 mM concentration. DNA solutions were prepared daily in a 10 mM Tris-HCl, 100 mM NaCl buffer (pH 8.5) and supplemented with DTT (final concentration: 1 mM). For the competition assay, compound solutions (diluted with buffer to *c* = 25 µM, 3 µL) or DMSO control (1:400 in buffer) were mixed with the substrate S (1.2 µM, 1 µL), placed in a thermostat at 37 °C, and MGMT (2.4 µM, 2 µL) was added. Final assay concentrations were as following: compounds, 12.5 µM; S, 200 nM; MGMT, 800 nM (excess enzyme was required to account for the incomplete activity); DMSO, 0.125% (v/v), in a total reaction volume of 6 µL. After 5 min at 37 °C, 1.5 µL of reaction mixtures were transferred to ice-cooled Eppendorf vials containing

the unlabeled reaction quencher Q (15 µM, 2.5 µL). Then, dH_2O (2 µL), 5X TANGO buffer (2 µL) and Bsp119I (Thermo Scientific, 2 U/mL, 2 µL) were added to each vial, and the vials were incubated at 37 °C for 1 h. The reactions were quenched by addition of formamide / 5 M aq. Na_2EDTA solution (80:20, 5 µL). Aliquots (10 µL) of each reaction were loaded into a 0.75-mm denaturing gel (15% polyacrylamide, 7 M urea) and separated at ambient temperature during 35 min (~1200 V, 20 W). Gels were visualized with a Typhoon 5 imager (GE Healthcare) using standard settings for Cy3 detection and quantified with ImageQuant TL software (GE Healthcare). Inhibition efficiency (%) was determined using Equation (3):

$$\text{Inhibition (\%)} = 100 \times \left(1 - \frac{R_{\text{comp}}}{R_{\text{control}}}\right), \quad (3)$$

where R_{comp} and R_{control} are relative amounts of the 10-mer reaction product (relative to the sum of the bands of the product and the 26-mer substrate, as determined by densitometry analysis of electrophoresis gels) for the compound and DMSO control, respectively.

For the endonuclease inhibition assay, the methylated substrate S was substituted by S′, and MGMT and Q where substituted by equal volumes of the Tris / DTT buffer; the experiments were performed and analyzed as above.

In the competitive assay, compound solutions (diluted with buffer to c = 50 µM, 1.5 µL) or DMSO control (2:400 in buffer) were mixed with CT DNA (160 µM bp, 1.5 µL) and incubated at room temperature for 10 min, followed by the addition of the substrate S (1.2 µM, 1 µL). The reaction vials were placed in a thermostat at 37 °C, and MGMT (2.4 µM, 2 µL) was added. The subsequent reaction (5 min), quenching and analysis steps were performed as described above. In the uncompetitive assays, solutions of MGMT (2.4 µM, 2 µL) and the compounds (25 µM, 3 µL) were preincubated for 30 min at room temperature, then placed in the thermostat (37 °C) and the substrate S (1.2 µM, 1 µL) was added. The subsequent reaction (5 min), quenching and analysis steps were performed as described above.

5.5. Cell culture experiments

General remarks: T98G human glioblastoma cell line was purchased from American Type Culture Collection (ATCC). Adherent cells were grown in Minimum Essential Medium (MEM 1X + GlutaMAX™, Life Technologies) supplemented with 1% penicillin/streptomycin (Life Technologies), 10% fetal bovine serum (Biowest) and 1% MEM Non-Essential Amino Acids Solution (MEM NEAA (100X), Life Technologies), kept in humidified atmosphere with 5% CO_2 in air at 37 °C and subcultured twice a week by dispersal with TrypLE™ Express Enzyme (Life Technologies).

Growth inhibition (GI_{50}) determination: Cells were seeded at (0.125–0.25) × 10^5 cells mL^{-1} in a 25 cm^2 flask between 3–4 days before the experiment in the conditions mentioned above. After reaching this time, the medium was removed and the cells were washed with 5 mL of sterile PBS. For each flask, 1 mL of TrypLE™ Express Enzyme (Life Technologies) were added to the flask for 5–10 minutes at 37 °C, followed by 9 mL of medium. Cells were counted using a MaxiZ™ counter (Orflo, Ketchum) and resuspended in media at a 0.125 × 10^5 cells mL^{-1} concentration. 200 µL of this suspension was added into each well of a 96-well plate (Costar). After 4 h, 1 µL of solution of compounds in DMSO were added such as to obtain the final drug concentration in a range from 0.015 to 25 µM (final concentration of DMSO in each well: 0.5% v/v) and mixed. The cells were incubated for 96 h in the conditions mentioned above. Cell viability was assessed by using CellTiter Glo® Luminescent Cell Viability Assay (Promega) following the kit instructions. Cells viability (V, %) was determined as the ratio of the luminescent signal of the cells treated with the compound(s) and the vehicle (DMSO, 0.5% v/v). Each condition was assayed at least three times with two technical replicates per plate.

For determination of viability through cell counting, the following protocol was employed: T98G cells were plated in 24-well tissue culture plates (TPP®) at 0.25 × 10^5 cells mL^{-1} in 1 mL medium, and 4 h later treated with varied concentrations of each compound and incubated for 96 h at 37 °C and 5% CO_2. After washing with 500 µL of PBS, 100 µL of TrypLE™ Express Enzyme (Life Technologies) was added to the cells for 5 min at 37 °C, followed by 900 µL of medium. Cells were counted as described before. Cells viability (%) were defined as the ratio between the concentration of cells treated with compound and the vehicle, where each condition was tested at least one time.

Drug combination experiments: Cells were seeded in a white 96-well tissue culture plate (Costar®) and the compounds were added as DMSO solutions and incubated for 2 h. After this time, TMZ was added as a DMSO solution, such as the final concentration of DMSO in each well was 0.5% v/v. The cells were grown for a total of 96 h and the experimental viability ($V_{exp,AB}$) was determined using CellTiter Glo® kit as described before. For the analysis in terms of Bliss Independence model [62,63], the theoretical viability of cells treated with a combination of drugs A and B ($V_{theo,AB}$) was calculated using Equation (4):

$$V_{theo,AB} = V_{exp,A} \times V_{exp,B}, \quad (4)$$

where $V_{exp,A}$ and $V_{exp,B}$ are the viabilities of cells treated individually with compounds A and B, respectively, at the same concentrations as in the combination experiment. The corresponding s.d. (σ) values were calculated using the error propagation formula, Equation (5):

$$\sigma^2 = (V_{Theo,AB})^2 \times \left(\frac{\sigma_{V_A}^2}{V_A^2} + \frac{\sigma_{V_B}^2}{V_B^2}\right), \quad (5)$$

where σ_{V_A} and σ_{V_B} are the s.d. values for the experimental viabilities $V_{exp,A}$ and $V_{exp,B}$, respectively. One-way ANOVA and Sidak post-test comparison statistical analysis were performed (GraphPad 6, www.graphpad.com) to compare $V_{theo,AB}$ with experimentally observed viability $V_{exp,AB}$.

For Combination Index (CI) determination, the Chou–Talalay method was used by employing CompuSyn software as per software manual (https://www.combosyn.com/) [65,66].

Inactivation of cellular MGMT: T98G cells were seeded at 0.125 × 10^5 cell mL^{-1} in 30 mL of media in T75 flasks and incubated as described before. After four days, media was removed, the flasks were washed with PBS (10 mL) and filled with fresh media containing DMSO (0.5% v/v) or the compounds (2 µM) and incubated for 2 h at 37 °C. Media was removed, and cells were washed with PBS (2 × 10 mL) and trypsinized collecting about 1 × 10^7 cells per treatment. The cells were pelleted and N_2-frozen for storing at −80 °C. The pellets were resuspended in the reaction buffer (50 mM Tris-HCl, 50 mM NaCl, 1 mM EDTA, 5% glycerol, pH 8.0) supplemented with DTT (1 mM) and 1X Halt™ protease cocktail (Thermo Scientific). The suspension was pulse-sonicated 5 times (5 s each, 30 s between pulses) at 4 °C and then centrifuged for 30 min at 4 °C and 14000 *g*; the supernatant was transferred to a clean tube and kept on ice. Protein concentration, measured using Pierce™ BCA protein assay kit (Thermo Scientific), was 4–8 mg mL^{-1}, similar to what is reported in the literature [54,67].

Reactions were performed in 150 µL of reaction mixture containing the protein extract (147.5 µL, 100–500 µg of protein) and DNA substrate S (2.5 µL of a 240 nM solution, final concentration: 4 nM) and incubated 2 h at 37 °C. DNA was extracted using phenol : chloroform : isoamyl alcohol (25:24:1, Sigma) saturated with 10 mM Tris and 1 mM EDTA, pH 8.0 (150 µL). 100 µL of the DNA-containing phase were employed to precipitate the DNA using 50 µL of NaOAc (3 M), 900 µL of cold abs. EtOH, 1 µL of glycogen (20 µg/µL, Invitrogen) and then stored at −20 °C overnight. The samples were centrifuged (2 h, 4 °C, 16,000 *g*) and the supernatant was carefully removed. The pellet was washed with 150 µL of cold 70% EtOH and re-centrifuged (10 min, 4 °C, 16,000 *g*). The supernatant was removed and the DNA was dried by speed vacuum, then dissolved in a total of 10 µL of solution containing H_2O (6 µL), 2 µL of 5X TANGO (2µL) and Bsp119I (2 U/mL, 2 µL). Gel electrophoresis analysis was carried as before and the activity was calculated by dividing the MGMT activity by the amount of total protein used for the assay. The results represent the mean ± s.d. of three independent biological experiments.

Live cell imaging: T98G cells were cultured as described above and plated in an 8-well plate (ibidi®) at 0.25 × 10^5 cells mL^{-1} in 0.3 mL medium, and 4 h later treated with compound **19a** (final concentration: 1.1 µM) and incubated for 96 h at 37 °C and 5% CO_2. Medium was

removed and the cells were washed with PBS (300 µL). Medium was replenished, DRAQ5™ (Invitrogen) was added as a nuclear dye (final concentration: 20 µM) and cells were incubated for 20 minutes at room temperature, protected from light. Finally, medium was removed; cells were washed and medium was added as before. Images were acquired on a TIRF Spinning Disk Microscope (Gataca systems, TiE Nikon), with a 100X oil magnification using a 488 nm laser (525 / 25 nm filter) and a 642 nm laser (700 / 75 nm filter). Pixel size was 0.11 µm and the *Z* step size was 0.5 µm over a Z range of 10 µm.

γ-H2AX immunostaining: T98G cells were plated in an 8-well plate Lab-Tek® II Chamber Slide™ at 0.125×10^5 cells mL^{-1} concentration for DMSO and TMZ treatment and at 0.25×10^5 cells mL^{-1} for the rest of the conditions in 0.4 mL of medium and treated 4 h later with DMSO, BG and **19a** for 2 h at 37 °C and 5% CO_2. Then, TMZ was added and cells were incubated in the same conditions for 94 h more. Medium was removed, and cells were washed with PBS (2 × 400 µL) and fixed with PFA (2% in PBS, 400 µL) for 10 min at rt, and then washed with PBS (3 × 400 µL). Cells were permeabilized with Triton X-100 (0.2% in PBS, 400 µL) for 10 min at room temperature and then washed with PBS (3 × 400 µL). Cells were incubated with goat serum (Abcam, 10 % in PBS, 250 µL) for 1 h at room temperature, washed once with PBS (400 µL) and incubated overnight with γ-H2AX antibody (MerckMillipore, Antiphospho-Histone H2A.X (Ser139), clone JBW301,1:500 in BSA 1%, 250 µL) at 4 °C. Cells were washed with PBS (5 × 400 µL, leaving for 5 min between washings) and incubated with the secondary antibody (Life Technologies, AlexaFluor™ 555 goat anti-mouse IgG1 (γ1), 1:600 in BSA 1%) for 30 min at room temperature. Cells were washed with PBS (5 × 400 µL, leaving for 5 minutes between washings) and slides were finally mounted with Vectashield® Mounting Medium for Fluorescence containing DAPI as nuclear dye (Vector Laboratories) and a cover glass (N° 1.5, VWR). Images were acquired on a 63X oil magnification with a Widefield Microscope (Leica) and processed using ImageJ software. Data presents the results of two individual replicate were a minimum of 150 cells were analyzed per condition.

Apoptosis and necrosis determination: T98G cells were incubated in a 6-well plate (TPP®) in a 5 mL final volume, at 0.35×10^5 cells mL^{-1} for DMSO and TMZ treatment and at 0.7×10^5 cells mL^{-1} for the rest of the conditions for the 48 h experiment, 0.25×10^5 cells mL^{-1} for DMSO and TMZ treatment, 0.5×10^5 cells mL^{-1} for **19a** and BG, and 1×10^5 cells mL^{-1} for the combination experiments for at 96 h. Cells were treated 4 h later with the compounds as DMSO solutions, incubated for 2 h at 37 °C and 5% CO_2 when TMZ was added and incubated to complete 48 h or 96 h of incubation. After this time, medium was removed and washed with PBS (2 mL), cells were trypsinized and counted. Medium was removed by centrifugation (5 min, 1500 *g* at 4 °C) and cells were washed again (2 × 2 mL) and analyzed using FITC Annexin V Apoptosis Detection Kit (BD Pharmagen™) according to the kit instructions. Cells were

analyzed with a BD FACSCanto II cytometer equipped with a 488 nm laser. The data presented were an average of three to five individual experiments per condition.

Caspase 3/7 activation assay: In a 96-well plate, T98G cells were seeded at 1×10^4 cells mL^{-1} for **19a** and **19a** / TMZ combination experiment and 0.5×10^4 cells mL^{-1} for DMSO and TMZ experiments. Compounds were added as for the combination assay experiments at the corresponding concentrations, namely DMSO (0.5% v/v), TMZ (94 µM), **19a** (1.1 µM) and **19a** / TMZ combination (1.1 and 94 µM, respectively). Cells were incubated with compounds for 96 h and caspase 3/7 activity was measured using the Caspase-Glo® 3/7 kit (Promega) as per kit instructions [92,93]. Values were normalized with respect to the DMSO control and the amount of total protein (considered proportional to the cell number). The results represent means ± s.d. from three independent biological replicates.

ACKNOWLEDGEMENTS

This work was supported by the European Union's Horizon 2020 research and Innovation programme under the Marie Skłodowska-Curie Grant Agreement No. 666003, through an IC-3i international PhD programme (PhD fellowship to JFP). The authors thank Dr. Michela Zuffo for the preliminary experiments related to MGMT inhibition.

REFERENCES

[1] J. Zhang, M.F.G. Stevens, T. D. Bradshaw, Temozolomide: Mechanisms of Action, Repair and Resistance, Curr. Mol. Pharmacol. 5 (2012) 102–114. doi:10.2174/1874467211205010102.

[2] T. Tykocki, M. Eltayeb, Ten-year survival in glioblastoma. A systematic review, J. Clin. Neurosci. 54 (2018) 7–13. doi:10.1016/j.jocn.2018.05.002.

[3] E.K. Liu, E.P. Sulman, P.Y. Wen, S.C. Kurz, Novel Therapies for Glioblastoma, Curr. Neurol. Neurosci. Rep. 20 (2020) 19. doi:10.1007/s11910-020-01042-6.

[4] S.Y. Lee, Temozolomide resistance in glioblastoma multiforme, Genes Dis. 3 (2016) 198–210. doi:10.1016/j.gendis.2016.04.007.

[5] D. Fu, J.A. Calvo, L.D. Samson, Balancing repair and tolerance of DNA damage caused by alkylating agents, Nat. Rev. Cancer. 12 (2012) 104–120. doi:10.1038/nrc3185.

[6] D.S. Daniels, T.T. Woo, K.X. Luu, D.M. Noll, N.D. Clarke, A.E. Pegg, J.A. Tainer, DNA binding and nucleotide flipping by the human DNA repair protein AGT, Nat. Struct. Mol. Biol. 11 (2004) 714–720. doi:10.1038/nsmb791.

[7] T. Helleday, E. Petermann, C. Lundin, B. Hodgson, R.A. Sharma, DNA repair pathways as targets for cancer therapy, Nat. Rev. Cancer. 8 (2008) 193–204. doi:10.1038/nrc2342.

[8] S. Jiapaer, T. Furuta, S. Tanaka, T. Kitabayashi, M. Nakada, Potential Strategies Overcoming the Temozolomide Resistance for Glioblastoma, Neurol. Med. Chir. (Tokyo). 58 (2018) 405–421. doi:10.2176/nmc.ra.2018-0141.

[9] M. Decker, ed., Design of Hybrid Molecules for Drug Development, Elsevier, 2017.

[10] Shaveta, S. Mishra, P. Singh, Hybrid molecules: The privileged scaffolds for various pharmaceuticals, Eur. J. Med. Chem. 124 (2016) 500–536. doi:10.1016/j.ejmech.2016.08.039.

[11] M. Rupp, Z.S. Mouhri, C. Williams, B.J. Jean-Claude, Molecular analysis of the dual targeting of the epidermal growth factor receptor and the O^6-methylguanine-DNA methyltransferase with a double arm hybrid molecule, Oncotarget. 9 (2018) 35041–35055. doi:10.18632/oncotarget.25120.

[12] Y. Wang, T. Ren, X. Lai, G. Sun, L. Zhao, N. Zhang, R. Zhong, Synthesis and Antitumor Activity Evaluation of a Novel Combi-nitrosourea Prodrug: BGCNU, ACS Med. Chem. Lett. 8 (2017) 174–178. doi:10.1021/acsmedchemlett.6b00358.

[13] G. Sun, N. Zhang, L. Zhao, T. Fan, S. Zhang, R. Zhong, Synthesis and antitumor activity evaluation of a novel combi-nitrosourea prodrug: Designed to release a DNA cross-linking agent and an inhibitor of O6-alkylguanine-DNA alkyltransferase, Bioorg. Med. Chem. 24 (2016) 2097–2107. doi:10.1016/j.bmc.2016.03.041.

[14] M.J. Wanner, M. Koch, G.J. Koomen, Synthesis and antitumor activity of methyltriazene prodrugs simultaneously releasing DNA-methylating agents and the antiresistance drug O 6-benzylguanine, J. Med. Chem. 47 (2004) 6875–

6883. doi:10.1021/jm049556d.

[15] R. Palchaudhuri, P.J. Hergenrother, DNA as a target for anticancer compounds: methods to determine the mode of binding and the mechanism of action, Curr. Opin. Biotechnol. 18 (2007) 497–503. doi:10.1016/j.copbio.2007.09.006.

[16] A. Ali, S. Bhattacharya, DNA binders in clinical trials and chemotherapy, Bioorg. Med. Chem. 22 (2014) 4506–4521. doi:10.1016/j.bmc.2014.05.030.

[17] K. Gurova, New hopes from old drugs: revisiting DNA-binding small molecules as anticancer agents, Futur. Oncol. 5 (2009) 1685–1704. doi:10.2217/fon.09.127.

[18] D.B. Oien, C.L. Pathoulas, U. Ray, P. Thirusangu, E. Kalogera, V. Shridhar, Repurposing quinacrine for treatment-refractory cancer, Semin. Cancer Biol. 68 (2021) 21–30. doi:10.1016/j.semcancer.2019.09.021.

[19] R. Ehsanian, C. Van Waes, S.M. Feller, Beyond DNA binding - a review of the potential mechanisms mediating quinacrine's therapeutic activities in parasitic infections, inflammation, and cancers, Cell Commun. Signal. 9 (2011) 13. doi:10.1186/1478-811X-9-13.

[20] R. Preet, P. Mohapatra, S. Mohanty, S.K. Sahu, T. Choudhuri, M.D. Wyatt, C.N. Kundu, Quinacrine has anticancer activity in breast cancer cells through inhibition of topoisomerase activity, Int. J. Cancer. 130 (2012) 1660–1670. doi:10.1002/ijc.26158.

[21] V. Di Bussolo, F. Minutolo, Curaxins: A New Family of Non-genotoxic Multitargeted Anticancer Agents, ChemMedChem. 6 (2011) 2133–2136. doi:10.1002/cmdc.201100476.

[22] K. V. Gurova, J.E. Hill, C. Guo, A. Prokvolit, L.G. Burdelya, E. Samoylova, A. V. Khodyakova, R. Ganapathi, M. Ganapathi, N.D. Tararova, D. Bosykh, D. Lvovskiy, T.R. Webb, G.R. Stark, A. V. Gudkov, Small molecules that reactivate p53 in renal cell carcinoma reveal a NF- B-dependent mechanism of p53 suppression in tumors, Proc. Natl. Acad. Sci. 102 (2005) 17448–17453. doi:10.1073/pnas.0508888102.

[23] C. Guo, A. V. Gasparian, Z. Zhuang, D.A. Bosykh, A.A. Komar, A. V. Gudkov, K. V. Gurova, 9-Aminoacridine-based anticancer drugs target the PI3K/AKT/mTOR, NF-κB and p53 pathways, Oncogene. 28 (2009) 1151–1161. doi:10.1038/onc.2008.460.

[24] T.S. Jani, J. DeVecchio, T. Mazumdar, A. Agyeman, J.A. Houghton, Inhibition of NF-κB signaling by quinacrine is cytotoxic to human colon carcinoma cell lines and is synergistic in combination with tumor necrosis factor-related apoptosis-inducing ligand (TRAIL) or Oxaliplatin, J. Biol. Chem. 285 (2010) 19162–19172. doi:10.1074/jbc.M109.091645.

[25] J.K.T. Dermawan, K. Gurova, J. Pink, A. Dowlati, S. De, G. Narla, N. Sharma, G.R. Stark, Quinacrine Overcomes Resistance to Erlotinib by Inhibiting FACT, NF-κB, and Cell-Cycle Progression in Non–Small Cell Lung Cancer, Mol. Cancer Ther. 13 (2014) 2203–2214. doi:10.1158/1535-7163.MCT-14-0013.

[26] A. V. Gasparian, C.A. Burkhart, A.A. Purmal, L. Brodsky, M. Pal, M. Saranadasa, D.A. Bosykh, M. Commane, O.A. Guryanova, S. Pal, A. Safina, S. Sviridov, I.E. Koman, J. Veith, A.A. Komar, A. V. Gudkov, K. V. Gurova,

Curaxins: Anticancer Compounds That Simultaneously Suppress NF- B and Activate p53 by Targeting FACT, Sci. Transl. Med. 3 (2011) 95ra74. doi:10.1126/scitranslmed.3002530.

[27] S. Dana, S.K. Keshri, J. Shukla, K.S. Vikramdeo, N. Mondal, P. Mukhopadhyay, S.K. Dhar, Design, Synthesis and Evaluation of Bifunctional Acridinine Naphthalenediimide Redox-Active Conjugates as Antimalarials, ACS Omega. 1 (2016) 318–333. doi:10.1021/acsomega.6b00060.

[28] P. Prasher, M. Sharma, Medicinal chemistry of acridine and its analogues, MedChemComm. 9 (2018) 1589–1618. doi:10.1039/C8MD00384J.

[29] P. Belmont, A. Boudali, J.F. Constant, M. Demeunynck, A. Fkyerat, P. Michon, G. Serratrice, J. Lhomme, Efficient and Versatile Chemical Tools for Cleavage of Abasic Sites in Dna, New J. Chem. 21 (1997) 47–54.

[30] P. Belmont, M. Jourdan, M. Demeunynck, J.F. Constant, J. Garcia, J. Lhomme, D. Carez, A. Croisy, Abasic site recognition in DNA as a new strategy to potentiate the action of anticancer alkylating drugs?, J. Med. Chem. 42 (1999) 5153–5159. doi:10.1021/jm9901428.

[31] S.C. Zimmerman, L.M. Luu, L. Nguyen, A.H. Jahromi, K.A. Miller, Y. Fu, A.M. Baranger, Developing Bivalent Ligands to Target CUG Triplet Repeats, the Causative Agent of Myotonic Dystrophy Type 1, J. Med. Chem. 56 (2013) 9471–9481. doi:10.1021/jm400794z.

[32] C.-H. Wong, Y. Fu, S.R. Ramisetty, A.M. Baranger, S.C. Zimmerman, Selective inhibition of MBNL1-CCUG interaction by small molecules toward potential therapeutic agents for myotonic dystrophy type 2 (DM2)., Nucleic Acids Res. 39 (2011) 8881–8890. doi:10.1093/nar/gkr415.

[33] G.H. Stein, T98G: An anchorage-independent human tumor cell line that exhibits stationary phase G1 arrest in vitro, J. Cell. Physiol. 99 (1979) 43–54. doi:10.1002/jcp.1040990107.

[34] M. Mohri, H. Nitta, J. Yamashita, Expression of multidrug resistance-associated protein (MRP) in human gliomas, J. Neurooncol. 49 (2000) 105–115. doi:10.1023/A:1026528926482.

[35] M.S. Bobola, S.H. Tseng, A. Blank, M.S. Berger, J. Silber, Role of O6-methylguanine-DNA methyltransferase in resistance of human brain tumor cell lines to the clinically relevant methylating agents temozolomide and streptozotocin, Clin. Cancer Res. 2 (1996) 735–741.

[36] M. Hermisson, A. Klumpp, W. Wick, J. Wischhusen, G. Nagel, W. Roos, B. Kaina, M. Weller, O6-methylguanine DNA methyltransferase and p53 status predict temozolomide sensitivity in human malignant glioma cells, J. Neurochem. 96 (2006) 766–776. doi:10.1111/j.1471-4159.2005.03583.x.

[37] I. Terashima, H. Kawate, K. Sakumi, M. Sekiguchi, K. Kohda, Substrate specificity of human O6-methylguanine-DNA methyltransferase for O6-benzylguanine derivatives in oligodeoxynucleotides, Chem. Res. Toxicol. 10 (1997) 1234–1239. doi:10.1021/tx9700580.

[38] G.T. Pauly, N.A. Loktionova, Q. Fang, S.L. Vankayala, W.C. Guida, A.E. Pegg, Substitution of aminomethyl at the meta-position enhances the inactivation of O6-alkylguanine-DNA alkyltransferase by O6- benzylguanine, J. Med. Chem. 51

(2008) 7144–7153. doi:10.1021/jm800675p.

[39] R.C. Moschel, M.G. McDougall, M.E. Dolan, L. Stine, A.E. Pegg, Structural Features of Substituted Purine Derivatives Compatible with Depletion of Human O6-Alkylguanine-DNA Alkyltransferase, J. Med. Chem. 35 (1992) 4486–4491. doi:10.1021/jm00101a028.

[40] R.C. Moschel, A.E. Pegg, Effect of O6-Benzylguanine Analogues on Sensitivity of Human Tumor Cells to the Cytotoxic Effects of Alkylating Agents, Cancer Res. 51 (1991) 3367–3372.

[41] G. Sun, T. Fan, N. Zhang, T. Ren, L. Zhao, R. Zhong, Identification of the Structural Features of Guanine Derivatives as MGMT Inhibitors Using 3D-QSAR Modeling Combined with Molecular Docking, Molecules. 21 (2016) 823. doi:10.3390/molecules21070823.

[42] A. Keppler, H. Pick, C. Arrivoli, H. Vogel, K. Johnsson, Labeling of fusion proteins with synthetic fluorophores in live cells, Proc. Natl. Acad. Sci. U. S. A. 101 (2004) 9955–9959. doi:10.1073/pnas.0401923101.

[43] A. Keppler, S. Gendreizig, T. Gronemeyer, H. Pick, H. Vogel, K. Johnsson, A general method for the covalent labeling of fusion proteins with small molecules in vivo, Nat. Biotechnol. 21 (2003) 86–89. doi:10.1038/nbt765.

[44] M.G. Ferlin, C. Marzano, G. Chiarelotto, F. Baccichetti, F. Bordin, Synthesis and antiproliferative activity of some variously substituted acridine and azacridine derivatives, Eur. J. Med. Chem. 35 (2000) 827–837. doi:10.1016/S0223-5234(00)00170-7.

[45] S.A. Ross, M. Pitié, B. Meunier, Synthesis of two acridine conjugates of the bis(phenanthroline) ligand “Clip-Phen” and evaluation of the nuclease activity of the corresponding copper complexes, Eur. J. Inorg. Chem. (1999) 557–563. doi:10.1002/(SICI)1099-0682(199903)1999:3<557::AID-EJIC557>3.0.CO;2-Y.

[46] W.J. Humphlett, C.R. Hauser, New Compounds. Certain Quinolyl and Acridyl Derivatives of β-Alanine, J. Am. Chem. Soc. 73 (1951). doi:10.1021/ja01150a600.

[47] R.S. McElhinney, D.J. Donnelly, J.E. McCormick, J. Kelly, A.J. Watson, J.A. Rafferty, R.H. Elder, M.R. Middleton, M.A. Willington, T.B.H. McMurry, G.P. Margison, Inactivation of O 6 -Alkylguanine-DNA Alkyltransferase. 1. Novel O 6-Hetarylmethyl)guanines Having Basic Rings in the Side Chain, J. Med. Chem. 41 (1998) 5265–5271. doi:10.1021/jm9708644.

[48] N.G. Lukyanenko, T.I. Kirichenko, S. V. Scherbakov, Novel cryptands containing thiourea units as a part of the macrocyclic framework, J. Chem. Soc. Perkin 1. 2 (2002) 2347–2351. doi:10.1039/b207902j.

[49] J.F. Constant, P. Laügaa, B.P. Roques, J. Lhommee, Heterodimeric Molecules Including Nucleic Acid Bases and 9-Aminoacridine: Spectroscopic Studies, Conformations, and Interactions with DNA, Biochemistry. 27 (1988) 3997–4003. doi:10.1021/bi00411a016.

[50] J. Bolte, C. Demuynck, M.F. Lhomme, J. Lhomme, J. Barbet, B.P. Roques, Synthetic Models Related to DNA Intercalating Molecules: Comparison between Quinacrine and Chloroquine in Their Ring-Ring Interaction with Adenine and Thymine, J. Am. Chem. Soc. 104 (1982) 760–765. doi:10.1021/ja00367a019.

[51] A.M. Brouwer, Standards for photoluminescence quantum yield measurements in solution (IUPAC Technical Report), Pure Appl. Chem. 83 (2011) 2213–2228. doi:10.1351/PAC-REP-10-09-31.

[52] H. Ihmels, K. Faulhaber, G. Viola, C. Schmuck, Evaluation of the DNA-Binding Properties of Cationic Dyes by Absorption and Emission Spectroscopy, in: C. Schmuck, H. Wennemers (Eds.), Highlights Bioorganic Chem. Methods Appl., Wiley-VCH Verlag GmbH & Co. KGaA, Weinheim, 2004: pp. 172–190. doi:10.1002/3527603727.ch2e.

[53] M. Eriksson, B. Nordén, Linear and circular dichroism of drug-nucleic acid complexes, in: Methods Enzymol., 2001: pp. 68–98. doi:10.1016/S0076-6879(01)40418-6.

[54] E.L. Kreklau, M. Limp-Foster, N. Liu, Y. Xu, M.R. Kelley, L.C. Erickson, A novel fluorometric oligonucleotide assay to measure O 6-methylguanine DNA methyltransferase, methylpurine DNA glycosylase, 8-oxoguanine DNA glycosylase and abasic endonuclease activities: DNA repair status in human breast carcinoma cells overexpressing , Nucleic Acids Res. 29 (2001) 2558–2566. doi:10.1093/nar/29.12.2558.

[55] Q. Qi, K. He, M.H. Yoo, C.B. Chan, X. Liu, Z. Zhang, J.J. Olson, G. Xiao, L. Wang, H. Mao, H. Fu, H. Tao, S.S. Ramalingam, S.Y. Sun, P.S. Mischel, K. Ye, Acridine yellow G blocks glioblastoma growth via dual inhibition of epidermal growth factor receptor and protein kinase C kinases, J. Biol. Chem. 287 (2012) 6113–6127. doi:10.1074/jbc.M111.293605.

[56] T. Marsoner, O.P. Schmidt, T. Triemer, N.W. Luedtke, DNA-Targeted Inhibition of MGMT, ChemBioChem. 18 (2017) 894–898. doi:10.1002/cbic.201600652.

[57] S.L. McGovern, B.T. Helfand, B. Feng, B.K. Shoichet, A Specific Mechanism of Nonspecific Inhibition, J. Med. Chem. 46 (2003) 4265–4272. doi:10.1021/jm030266r.

[58] A.E. Pegg, L. Chung, R.C. Moschel, Effect of DNA on the inactivation of O6-alkylguanine-DNA alkyltransferase by 9-substituted O6-benzylguanine derivatives, Biochem. Pharmacol. 53 (1997) 1559–1564. doi:10.1016/S0006-2952(97)00060-9.

[59] Promega Corporation, CellTiter-Glo® Luminescent Cell Viability Assay, (2016) 1–14.

[60] M.E. Dolan, R.C. Moschel, A.E. Pegg, Depletion of mammalian O6-alkylguanine-DNA alkyltransferase activity by O6-benzylguanine provides a means to evaluate the role of this protein in protection against carcinogenic and therapeutic alkylating agents, Proc. Natl. Acad. Sci. U. S. A. 87 (1990) 5368–5372. doi:10.1073/pnas.87.14.5368.

[61] K.H. Tomaszowski, R. Schirrmacher, B. Kaina, Multidrug Efflux Pumps Attenuate the Effect of MGMT Inhibitors, Mol. Pharm. 12 (2015) 3924–3934. doi:10.1021/acs.molpharmaceut.5b00341.

[62] E. Demidenko, T.W. Miller, Statistical determination of synergy based on Bliss definition of drugs independence, PLoS One. 14 (2019) 1–22. doi:10.1371/journal.pone.0224137.

[63] J. Foucquier, M. Guedj, Analysis of drug combinations: current methodological

landscape, Pharmacol. Res. Perspect. 3 (2015) e00149. doi:10.1002/prp2.149.

[64] K.R. Roell, D.M. Reif, A.A. Motsinger-Reif, An Introduction to Terminology and Methodology of Chemical Synergy—Perspectives from Across Disciplines, Front. Pharmacol. 8 (2017) 158. doi:10.3389/fphar.2017.00158.

[65] T.C. Chou, Drug combination studies and their synergy quantification using the chou-talalay method, Cancer Res. 70 (2010) 440–446. doi:10.1158/0008-5472.CAN-09-1947.

[66] T.C. Chou, Theoretical basis, experimental design, and computerized simulation of synergism and antagonism in drug combination studies, Pharmacol. Rev. 58 (2006) 621–681. doi:10.1124/pr.58.3.10.

[67] A.A. Beharry, Z.D. Nagel, L.D. Samson, E.T.K. Kool, Fluorogenic real-time reporters of DNA repair by MGMT, a clinical predictor of antitumor drug response, PLoS One. 11 (2016) 1–15. doi:10.1371/journal.pone.0152684.

[68] W.M. Bonner, C.E. Redon, J.S. Dickey, A.J. Nakamura, O.A. Sedelnikova, S. Solier, Y. Pommier, γH2AX and cancer, Nat. Rev. Cancer. 8 (2008) 957–967. doi:10.1038/nrc2523.

[69] C.B. Jackson, S.I. Noorbakhsh, R.K. Sundaram, A.N. Kalathil, S. Ganesa, L. Jia, H. Breslin, D.M. Burgenske, O. Gilad, J.N. Sarkaria, R.S. Bindra, Temozolomide sensitizes MGMT-deficient tumor cells to ATR inhibitors, Cancer Res. 79 (2019) 4331–4338. doi:10.1158/0008-5472.CAN-18-3394.

[70] Z. Yang, D. Wei, X. Dai, M.F.G. Stevens, T.D. Bradshaw, Y. Luo, J. Zhang, C8-Substituted Imidazotetrazine Analogs Overcome Temozolomide Resistance by Inducing DNA Adducts and DNA Damage, Front. Oncol. 9 (2019) 485. doi:10.3389/fonc.2019.00485.

[71] Y. Sato, A. Kurose, A. Ogawa, K. Ogasawara, F. Traganos, Z. Darzynkiewicz, T. Sawai, Diversity of DNA damage response of astrocytes and glioblastoma cell lines with various p53 status to treatment with etoposide and temozolomide, Cancer Biol. Ther. 8 (2009) 452–457. doi:10.4161/cbt.8.5.7740.

[72] Z. Yang, D. Wei, X. Dai, M.F.G. Stevens, T.D. Bradshaw, Y. Luo, J. Zhang, C8-Substituted Imidazotetrazine Analogs Overcome Temozolomide Resistance by Inducing DNA Adducts and DNA Damage, Front. Oncol. 9 (2019) 485. doi:10.3389/fonc.2019.00485.

[73] K. Alarcon, M. Demeunynck, J. Lhomme, D. Carrez, A. Croisy, Potentiation of BCNU Cytotoxicity by Molecules Targeting Abasic Lesions in DNA, Bioorg. Med. Chem. 9 (2001) 1901–1910. doi:10.1016/S0968-0896(01)00097-9.

[74] K. Alarcon, M. Demeunynck, J. Lhomme, D. Carrez, A. Croisy, Diaminopurine-acridine heterodimers for specific recognition of abasic site containing DNA. Influence on the biological activity of the position of the linker on the purine ring, Bioorg. Med. Chem. Lett. 11 (2001) 1855–1858. doi:10.1016/S0960-894X(01)00310-9.

[75] K. Benner, A. Granzhan, H. Ihmels, G. Viola, Targeting Abasic Sites in DNA by Aminoalkyl-Substituted Carboxamidoacridizinium Derivatives and Acridizinium–Adenine Conjugates, Eur. J. Org. Chem. (2007) 4721–4730. doi:10.1002/ejoc.200700207.

[76] M. Chakravarty, P. Ganguli, M. Murahari, R.R. Sarkar, G.J. Peters, Y.C. Mayur, Study of Combinatorial Drug Synergy of Novel Acridone Derivatives With Temozolomide Using in-silico and in-vitro Methods in the Treatment of Drug-Resistant Glioma, Front. Oncol. 11 (2021) 625899. doi:10.3389/fonc.2021.625899.

[77] M. Melikishvili, D.W. Rodgers, M.G. Fried, 6-Carboxyfluorescein and structurally similar molecules inhibit DNA binding and repair by O6-alkylguanine DNA alkyltransferase, DNA Repair. 10 (2011) 1193–1202. doi:10.1016/j.dnarep.2011.09.007.

[78] B.I. Escher, L. Henneberger, M. König, R. Schlichting, F.C. Fischer, Cytotoxicity Burst? Differentiating Specific from Nonspecific Effects in Tox21 in Vitro Reporter Gene Assays, Environ. Health Perspect. 128 (2020) 077007. doi:10.1289/EHP6664.

[79] T. Johannessen, M.M. Hasan-Olive, H. Zhu, O. Denisova, A. Grudic, M.A. Latif, H. Saed, J.K. Varughese, G.V. Røsland, N. Yang, T. Sundstrøm, A. Nordal, K.J. Tronstad, J. Wang, M. Lund-Johansen, A. Simonsen, B. Janji, J. Westermarck, R. Bjerkvig, L. Prestegarden, Thioridazine inhibits autophagy and sensitizes glioblastoma cells to temozolomide, Int. J. Cancer. 144 (2019) 1735–1745. doi:10.1002/ijc.31912.

[80] C. Felip-León, O. Martínez-Arroyo, S. Díaz-Oltra, J.F. Miravet, N. Apostolova, F. Galindo, Synthesis, spectroscopic studies and biological evaluation of acridine derivatives: The role of aggregation on the photodynamic efficiency, Bioorg. Med. Chem. Lett. 28 (2018) 869–874. doi:10.1016/j.bmcl.2018.02.005.

[81] A. Lim, B.F.L. Li, The nuclear targeting and nuclear retention properties of a human DNA repair protein O6-methylguanine-DNA methyltransferase are both required for its nuclear localization: the possible implications., EMBO J. 15 (1996) 4050–4060. doi:10.1002/j.1460-2075.1996.tb00778.x.

[82] M. Belanich, T. Randall, M.A. Pastor, J.T. Kibitel, L.G. Alas, M.E. Dolan, S.C. Schold, M. Gander, F.J. Lejeune, B.F.L. Li, A.B. White, P. Wasserman, M.L. Citron, D.B. Yarosh, Intracellular localization and intercellular heterogeneity of the human DNA repair protein O6-methylguanine-DNA methyltransferase, Cancer Chemother. Pharmacol. 37 (1996) 547–555. doi:10.1007/s002800050427.

[83] A. Daina, O. Michielin, V. Zoete, SwissADME: A free web tool to evaluate pharmacokinetics, drug-likeness and medicinal chemistry friendliness of small molecules, Sci. Rep. 7 (2017) 1–13. doi:10.1038/srep42717.

[84] H. Liu, L. Wang, M. Lv, R. Pei, P. Li, Z. Pei, Y. Wang, W. Su, X.-Q. Xie, AlzPlatform: An Alzheimer's Disease Domain-Specific Chemogenomics Knowledgebase for Polypharmacology and Target Identification Research, J. Chem. Inf. Model. 54 (2014) 1050–1060. doi:10.1021/ci500004h.

[85] C.D. Arvanitis, G.B. Ferraro, R.K. Jain, The blood–brain barrier and blood–tumour barrier in brain tumours and metastases, Nat. Rev. Cancer. 20 (2020) 26–41. doi:10.1038/s41568-019-0205-x.

[86] E. Belykh, K. V. Shaffer, C. Lin, V.A. Byvaltsev, M.C. Preul, L. Chen, Blood-Brain Barrier, Blood-Brain Tumor Barrier, and Fluorescence-Guided Neurosurgical Oncology: Delivering Optical Labels to Brain Tumors, Front.

Oncol. 10 (2020) 1–27. doi:10.3389/fonc.2020.00739.

[87] S. Bonse, C. Santelli-Rouvier, J. Barbe, R.L. Krauth-Siegel, Inhibition of Trypanosoma cruzi trypanothione reductase by acridines: Kinetic studies and structure-activity relationships, J. Med. Chem. 42 (1999) 5448–5454. doi:10.1021/jm990386s.

[88] C.C. Ward, J.I. Kleinman, S.M. Brittain, P.S. Lee, C.Y.S. Chung, K. Kim, Y. Petri, J.R. Thomas, J.A. Tallarico, J.M. McKenna, M. Schirle, D.K. Nomura, Covalent Ligand Screening Uncovers a RNF4 E3 Ligase Recruiter for Targeted Protein Degradation Applications, ACS Chem. Biol. 14 (2019) 2430–2440. doi:10.1021/acschembio.8b01083.

[89] Z. Lijiao, P. Ruizeng, R. Ting, Z. Rugang, Z. Hufen, Low-oxygen activated joint chloroethane nitrourea compound and preparation method and application, 2016.

[90] W.C. Tse, D.L. Boger, A Fluorescent Intercalator Displacement Assay for Establishing DNA Binding Selectivity and Affinity, Acc. Chem. Res. 37 (2004) 61–69. doi:10.1021/ar030113y.

[91] C.L. Chan, Z.N. Wu, T. Ciardelli, A. Eastman, E. Bresnick, Kinetic and DNA-Binding Properties of Recombinant Human O6-Methylguanine-DNA Methyltransferase, Arch. Biochem. Biophys. 300 (1993) 193–200. doi:10.1006/abbi.1993.1027.

[92] Promega Corporation, Caspase-Glo ® 3/7 Assay, 2015.

[93] T. Xu, C. Niu, X. Zhang, M. Dong, β-Ecdysterone protects SH-SY5Y cells against β-amyloid-induced apoptosis via c-Jun N-terminal kinase-and Akt-associated complementary pathways, Lab. Investig. 98 (2018) 489–499. doi:10.1038/s41374-017-0009-0.